iScience

CellPress
OPEN ACCESS

Article

Structural basis of the IL-1 receptor TIR domain-mediated IL-1 signaling

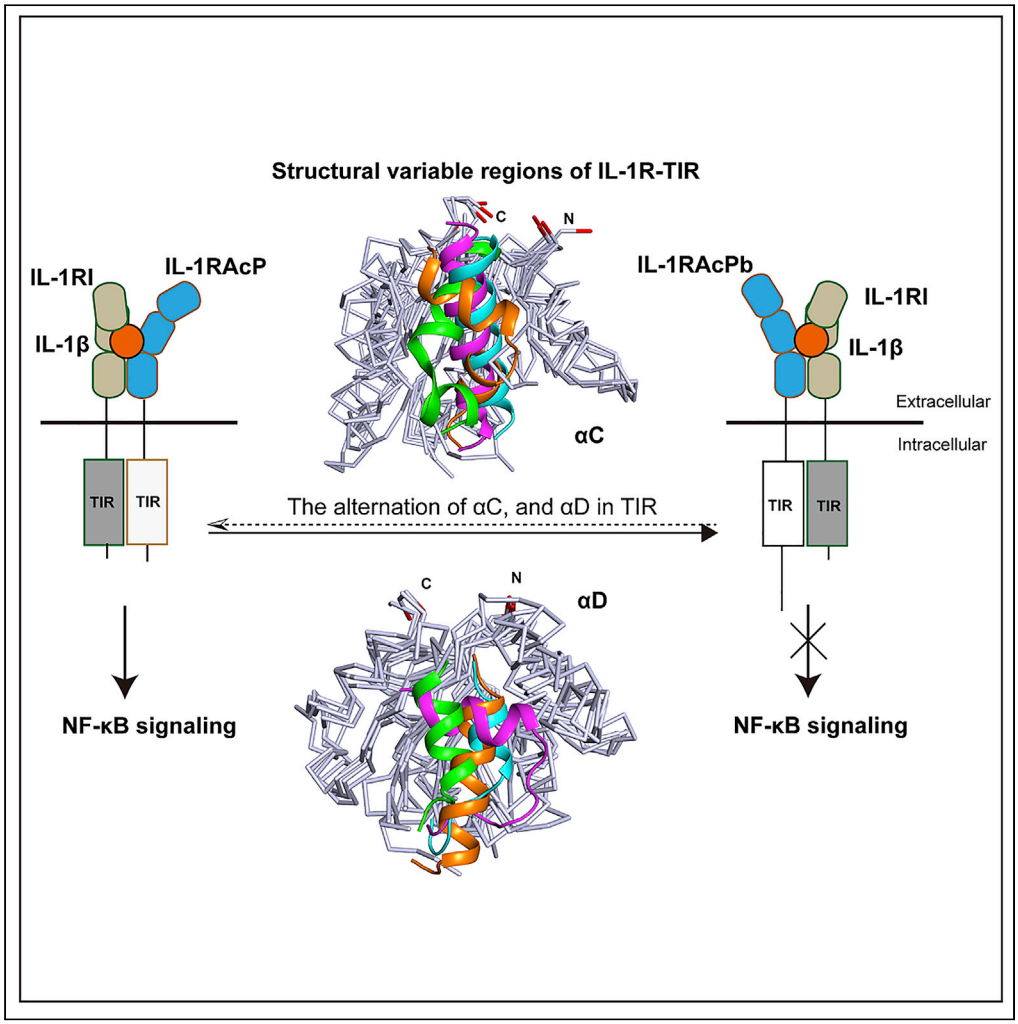

Jianjie Zhou, Yu Xiao, Yifei Ren, Jiwan Ge, Xinquan Wang

xinquanwang@mail.tsinghua.edu.cn

Highlights

The crystal structures of several IL-1R TIR domains were determinated

Structurally variant regions in TIR domains were revealed by structural comparisons

Differential TIR domain determines signaling discrepancy between IL-1RAcP and IL-1RAcPb

αC/αD regions and several residues there were proved to be vital for IL-1 signaling

Zhou et al., iScience 25, 104508
July 15, 2022
https://doi.org/10.1016/j.isci.2022.104508

iScience

CellPress
OPEN ACCESS

Article

Structural basis of the IL-1 receptor TIR domain-mediated IL-1 signaling

Jianjie Zhou,[1] Yu Xiao,[1] Yifei Ren,[1] Jiwan Ge,[1] and Xinquan Wang[1,2,*]

SUMMARY

The cytoplasmic Toll/interleukin-1 receptor (TIR) domains of IL-1 receptors (IL-1Rs) are evolutionally conserved and essential for transmitting signals. IL-1RAcP is a shared co-receptor in the IL-1R family for signaling. Its splicing form IL-1RAcPb contains a different TIR domain and is unable to transduce NF-κB signaling. Here, we determined crystal structures of TIR domains of IL-1RAcPb and other IL-1Rs including IL-18Rβ, IL-1RAPL2, and zebrafish SIGIRR (zSIGIRR). Structurally variant regions in the TIR domain important for signaling were revealed by structural comparisons. Taking advantage of the IL-1RAcP/IL-1RAcPb pair, we demonstrated that differential TIR domain determines signaling discrepancies between IL-1RAcP and IL-1RAcPb. We also proved the functional importance of two helices (αC and αD) in the structurally variable regions and pinpointed critical residues in αC and αD for signaling. These results collectively provide additional and important knowledge for fully understanding the molecular basis of IL-1R TIR domain in mediating signaling.

INTRODUCTION

The IL-1 family cytokines play important roles in both innate and adaptive immune responses, and are involved in a variety of immune and inflammatory diseases, or even cancer (Dinarello, 2009; Narayanan and Park, 2015; Sims and Smith, 2010). These eleven cytokines include seven agonists (IL-1α, IL-1β, IL-18, IL-33, IL-36α, IL-36β, and IL-36γ), three receptor antagonists (IL-1Ra, IL-36Ra, and IL-38), and one anti-inflammatory cytokine IL-37 (Fields et al., 2019). The representative IL-1β, one of the earliest studied interleukins, is a strong inflammatory cytokine, mediating non-specific effects in inflammatory responses, activating immune cells, and inducing the expression and secretion of inflammatory cytokines and chemokines (Gabay et al., 2010). The IL-1 family cytokines exert active functions by binding to the corresponding IL-1 receptors (IL-1R) on the surface of target cells. The IL-1R family members, belonging to the Toll/IL-1 receptor (TIR) domain receptor superfamily, are single-pass transmembrane proteins (Boraschi and Tagliabue, 2006). Their extracellular part, which is responsible for the recognition of cytokines and the assembly of cytokine/receptor signaling complexes, usually contains three Ig-like domains, while their intracellular part contains a TIR domain crucial for downstream signal transduction (Boraschi et al., 2018). There are ten members in the IL-1R family, comprising primary receptors IL-1RI (also known as IL-1R1), IL-1RII (IL-1R2), ST2 (IL-1R4), IL-1Rrp2 (IL-1R6), and IL-18Rα (IL-1R5), co-receptors IL-1RAcP (IL-1R3) and IL-18Rβ (IL-1R7), inhibitory receptor SIGIRR (IL-1R8), and two orphan receptors IL-1RAPL1 (IL-1R9) and IL-1RAPL2 (IL-1R10) (Boraschi et al., 2018). The signal transduction pathway starts with the recognition of IL-1 agonist by the primary receptor and the subsequent recruitment of the co-receptor. These two receptors then juxtapose their intracellular TIR domains and bind cytosolic adaptors such as myeloid differentiation primary response protein 88 (MyD88), triggering a cascade of kinases and finally activating the NF-κB and MAPK signaling (Dinarello, 2009). For example, IL-1β binds to its primary receptor IL-1RI and then recruits the co-receptor IL-1RAcP to form a signaling-competent ternary complex IL-1β/IL-1RI/IL-1RAcP (Dinarello, 2009). Other signaling complexes in the family include the IL-1α/IL-1RI/IL-1RAcP, IL-33/ST2/IL-1RAcP, IL-36α/IL-1Rrp2/IL-1RAcP, IL-36β/IL-1Rrp2/IL-1RAcP, IL-36γ/IL-1Rrp2/IL-1RAcP, and IL-18/IL-18Rα/IL-18Rβ (Dinarello, 2009; Garlanda et al., 2013; Sims and Smith, 2010). As a shared co-receptor, IL-1RAcP not only mediates the signal transduction of agonists IL-1α, IL-1β, IL-33, IL-36α, IL-36β, and IL-36γ but also is involved in forming non-signaling ternary complexes such as IL-1α/IL-1RII/IL-1RAcP and IL-1β/IL-1RII/IL-1RAcP for negative regulation (Dinarello, 2009; Garlanda et al., 2013; Sims and Smith, 2010).

IL-1RAcP is widely expressed in various types of cells including neurons and glial cells in the nervous system, reflecting its important roles in mediating and regulating the activities of the IL-1 family cytokines (Smith

[1]The Ministry of Education Key Laboratory of Protein Science, Beijing Advanced Innovation Center for Structural Biology, Beijing Frontier Research Center for Biological Structure, Collaborative Innovation Center for Biotherapy, School of Life Sciences, Tsinghua University, Beijing 100084, China

[2]Lead contact

*Correspondence: xinquanwang@mail.tsinghua.edu.cn

https://doi.org/10.1016/j.isci.2022.104508

et al., 2009; Yabuuchi et al., 1994). There exists a splice isoform of IL-1RAcP, namely IL-1RAcPb (IL-1R3b), whose expression is restricted in the CNS (mainly in neuronal cells) (Huang et al., 2011; Smith et al., 2009). Current studies indicate that IL-1RAcPb plays an important role in regulating the response of the CNS to IL-1β (Gosselin et al., 2013; Huang et al., 2011; Nguyen et al., 2011; Prieto et al., 2015; Smith et al., 2009). For example, IL-1RAcPb is able to modulate the activity of MAPK p38 with the presence of IL-1RAcP in neurons and it was also shown to induce Src phosphorylation and to enhance N-methyl-D-aspartate (NMDA)-induced calcium influx in neurons (Huang et al., 2011). However, IL-1RAcPb was shown to be unable to mediate the NF-κB activation, although it is able to form a ternary complex with IL-1β/IL-1RI like IL-1RAcP (Smith et al., 2009). Owing to the distinct usage of the last exon, IL-1RAcP and IL-1RAcPb differ in the intracellular TIR domain and the C-terminal tail that follows it (Smith et al., 2009). Considering their function discrepancies, IL-1RAcP and its isoform IL-1RAcPb form a good receptor pair for the study of the IL-1R TIR domain and the C-terminal tail in mediating and modulating the IL-1 signaling.

The complex structures of IL-1β, IL-1Ra, IL-18, and IL-33 bound by their receptor extracellular domains have been determined (Gunther et al., 2017; Liu et al., 2013; Schreuder et al., 1997; Thomas et al., 2012; Tsutsumi et al., 2014; Vigers et al., 1997; Wang et al., 2010; Wei et al., 2014), providing important insights into extracellular ligand recognition and receptor assembly in the IL-1/IL-1R family. However, our structural knowledge about the IL-1R TIR domain is extremely limited, with only the reported crystal structure of the orphan receptor IL-1RAPL1 TIR domain (Khan et al., 2004). The IL-1R TIR domains are supposed to share structural fold and signaling mechanisms, but the relatively low sequence identities in the range of 25%–37% (except for 74% of that between IL-1RAPL1-TIR and IL-1RAPL2-TIR) indicate important differences in determining their specificities. Here, we determined the crystal structure of the IL-1RAcPb TIR domain, as well as the TIR domains of other IL-1Rs including IL-18Rβ, IL-1RAPL2, SIGIRR, and its mutant SIGIRR-C299S. Structural comparisons of these IL-1R TIR domains suggest key functional segments in mediating NF-κB activation, which were further confirmed by mutagenesis and luciferase assay using the IL-1RAcP/IL-1RAcPb receptor pair. Our results collectively provide additional structural and biochemical knowledge for fully understanding the molecular basis of the IL-1R TIR domain in mediating signaling.

RESULTS

Structure determination and analyses of the IL-1R TIR domain

To explore the mechanism by which the IL-1R TIR domain exerts its signal transduction function, we first attempted to determinate the crystal structures of multiple TIR domains of this family, especially the core co-receptor IL-1RAcP and its alternative splicing form IL-1RAcPb. Although we tried several constructs with variant domain boundaries and different expression systems, the recombinant IL-1RAcP-TIR always had a strong tendency of aggregation to prevent crystallization. In contrast, the IL-1RAcPb-TIR was expressed and purified with good biochemical properties and its crystal structure was determined at 2.14 Å resolution (Table 1). We also successfully determined the crystal structures of the TIR domains of IL-18Rβ (1.88 Å), IL-1RAPL2 (2.99 Å), and zebrafish SIGIRR (zSIGIRR-TIR, 3.04 Å) and its mutant zSIGIRR-C299S-TIR (1.88 Å) (Table 1). IL-1RAcPb-TIR, IL-1RAPL2-TIR, and IL-18Rβ-TIR are all monomeric in solution, and in their crystal structures, the asymmetric unit contains one IL-1RAcPb-TIR, one IL-1RAPL2-TIR, and four IL-18Rβ-TIR molecules, respectively. The zSIGIRR-TIR exhibited both dimer and monomer in solution. For the three molecules in the crystal asymmetric unit, two are linked by an inter-chain disulfide bond C299-C299. When this cysteine was mutated to serine, the zSIGIRR-C299S-TIR was monomer in solution and there is one molecule in the crystal asymmetric unit. The monomeric zSIGIRR-TIR and zSIGIRR-C299S-TIR structures are nearly identical (Figure S1). Therefore, we utilized IL-1RAcPb-TIR, IL-18Rβ-TIR, IL-1RAPL2-TIR, and zSIGIRR-TIR for the following structural analyses and comparison. These four TIR domains all adopt a typical fold with five parallel β-strands surrounded by five helices, named βA-αA-βB-αB-βC-αC-βD-αD-βE-αE from the N- to C-terminus, which are connected with loops including AA, AB, BB, BC, CC, CD, DD, DE, and EE (Figure 1A).The DALI sever was used to compare structures of the IL-1R TIR domains, containing the previously reported structure of the IL-1RAPL1-TIR, and the relevant parameters were presented, including *Z* score, RMSD value, lali, nres, and identity (Holm, 2020) (Table S1). Structural comparisons among them show that the helix αC has three different orientations among the IL-1R TIR domains. Specifically, IL-1RAcPb-TIR and IL-18Rβ-TIR are similar by comprising a continuous αC helix (Figure 1A). In contrast, IL-1RAPL1 and IL-1RAPL2 TIR domains are similar by having a discontinuous αC helix with a 90° turn in the middle (Figures 1A and 1B). Although zSIGIRR-TIR also has a continuous αC helix, it has a positional angle difference from the αC of IL-1RAcPb-TIR after overall structural alignment (Figures 1A and 1B). The αD is another structurally variable region among the IL-1R TIR domains (Figure 1A).

Table 1. Diffraction data and structure refinement

	IL-1RAcPb-TIR	IL-18Rβ-TIR	IL-1RAPL2-TIR	zSIGIRR-C299S-TIR	zSIGIRR-TIR
Data collection					
Space group	$P2_12_12_1$	$P\ 2_1$	$P\ 4_3\ 2_1\ 2$	$P\ 2_1\ 2_1\ 2_1$	$C\ 2\ 2\ 2$
Cell dimensions					
a, *b*, *c* (Å)	34.63, 51.17, 78.48	39.76, 161.07, 52.16	51.14, 51.14, 184.78	31.74, 61.61, 69.53	84.00, 145.36, 75.66
α, β, γ (°)	90, 90, 90	90, 112.44, 90	90, 90, 90	90, 90, 90	90, 90, 90
Resolution (Å)	50.00–2.14 (2.19–2.14)[a]	50.00–1.88 (1.92–1.88)	49.29–2.99 (3.15–2.99)	50.00–1.88 (1.92–1.88)	50.00–3.04 (3.09–3.04)
R_{sym} or R_{merge}	0.13 (0.76)	0.08(0.50)	0.16(1.72)	0.13(0.54)	0.09(0.69)
Mean I/sigma(I)	13.4 (1.7)	13.0(0.9)	19.6(3.1)	13.0(1.4)	11.1(2.6)
Completeness (%)	97.25 (84.67)	95.61 (83.56)	99.8(100.0)	91.83 (57.42)	99.8(100.0)
Redundancy	10.3 (5.1)	4.6(2.6)	24.0(26.3)	9.2(2.9)	10.3(10.9)
Refinement					
No. reflections	7,875 (663)	46,801 (4,060)	5,452 (515)	10,663 (631)	9,184(455)
R_{work}/R_{free} (%)	19.99/24.31	18.64/22.26	24.03/28.25	19.77/23.92	23.88/27.33
No. atoms (Protein)	1,184	4,616	1,289	1,225	3,623
B-factors (Å^2) (Protein)	34.57	35.45	87.42	22.91	74.0
R.m.s. deviations					
Bond lengths (Å)	0.007	0.010	0.012	0.009	0.012
Bond angles (°)	0.90	1.37	1.49	1.08	1.43
Ramachandran plot (%)					
Favored	98.6	96.0	92.1	98.0	95.8
Allowed	0.69	3.60	6.62	2.05	3.01
Outliers	0.69	0.36	1.32	0.00	1.16

One crystal for the data.
[a]Values in parentheses are for highest resolution shell.

IL-1RAPL1-TIR and IL-1RAPL2-TIR have a relatively long and continuous αD, zSIGIRR-TIR has a nearly 180° kinked αD, and IL-1RAcPb-TIR has a short αD. The αD of IL-18Rβ-TIR is unique by adopting a position that is almost perpendicular to those of other IL-1R TIR αD helices. Of note, the αD of IL-18Rβ-TIR is more structurally similar to the TLR TIR domains (Jang and Park, 2014; Nyman et al., 2008; Xu et al., 2000) than other IL-1R TIR domains (Figure S2). In the TLR family, although there are some local structural variations in the TIR domain structure (mainly in the αC and nearby regions) (Figure S2), their overall conformation similarity is higher than that among IL-1R TIR domains, which also correspond to the higher sequence identity of the TIR domains in the TLR family than in the IL-1R family. The sequence identities are more than 50% among the TLR TIR domains, and that between TLR1-TIR and TLR6-TIR is as high as 87%.

The variant TIR domain determines the inability of IL-1RAcPb in mediating NF-κB activation

Owing to the usage of the exon 12b instead of exon 12, IL-1RAcPb differs from IL-1RAcP in two regions: the TIR domain and the C-terminal tail that follows it (Smith et al., 2009) (Figure 2A). Sequence alignment showed that IL-1RAcPb and IL-1RAcP are identical in the extracellular part and the transmembrane region (Figure S3). Their TIR domains are different in the C-terminal region encoded by exon 12 in the IL-1RAcP and by exon 12b in the IL-1RAcPb, and the amino acid sequence identity in this region is only 35% (Figures 3A and S3). In addition, after the TIR domain, the C-terminal tail in the IL-1RAcPb (~140 residues) is much longer than that (~24 residues) in the IL-1RAcP (Figure S3). It has been reported that IL-1RAcPb binds to the IL-1/IL-1RI binary complex to form a ternary complex, but it cannot mediate the canonical IL-1 signaling. Therefore, we utilized the IL-1RAcP/IL-1RAcPb pair to explore the structure-function relationship of the TIR domain.

We first explored whether the C-terminal long tail in the IL-1RAcPb exerts an inhibitory effect on signal transduction. To this end, we constructed a clone of IL-1RAcPb with its C-terminal tail deleted

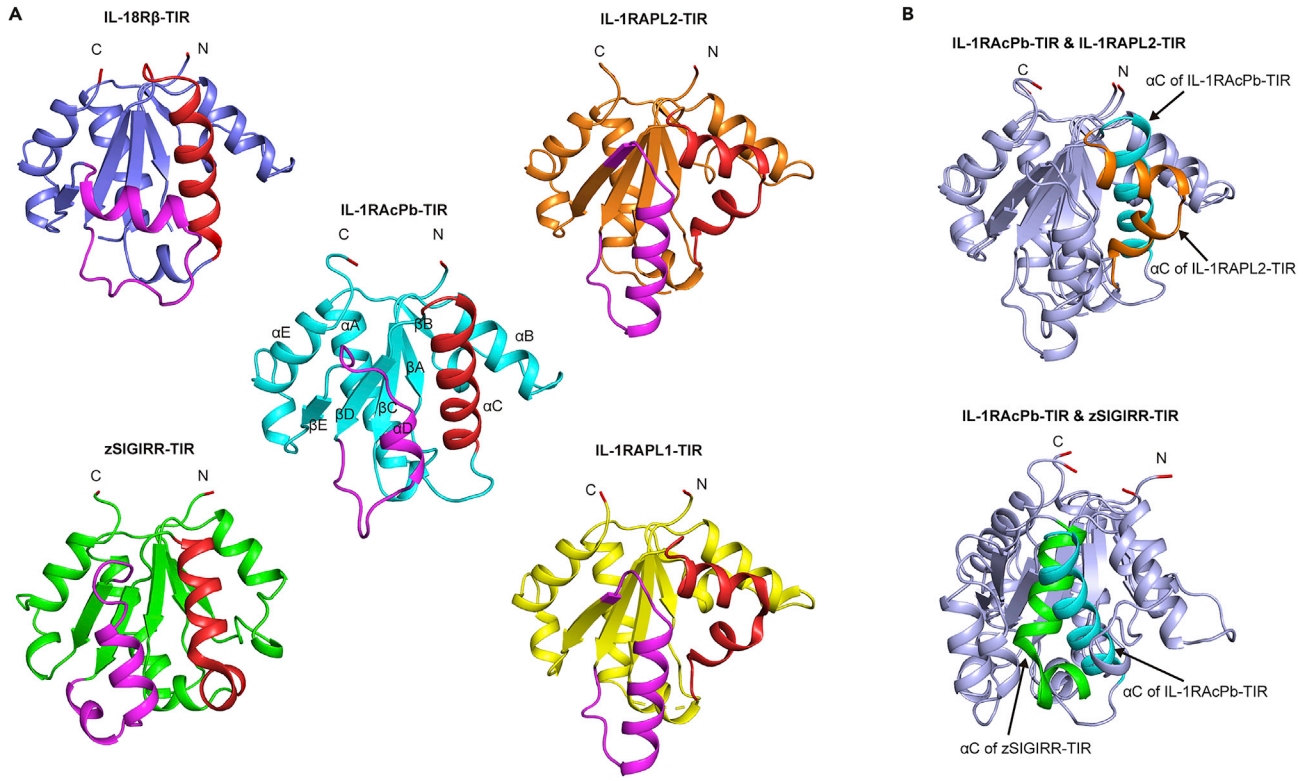

Figure 1. Crystal structures of TIR domains of several IL-1R family members and their comparisons

(A) Shown are the cartoon figures of monomeric TIR domain structures of IL-1RAcPb (cyan), IL-18Rβ (slate), IL-1RAPL2 (tv_orange), IL-1RAPL1 (PDB ID: 1T3G, yellow), and zSIGIRR (green). With IL-1RAcPb-TIR as an example, its secondary structure elements are labeled according to the convention of Xu et al. (2000). αC and αD regions of all these members are labeled red and magenta, respectively. These structures are all presented in analogous orientations.

(B) Cartoon representation of the superposition of the TIR domains from IL-1RAcPb and IL-1RAPL2/zSIGIRR. The αC helix of IL-1RAcPb-TIR, IL-1RAPL2, and zSIGIRR-TIR are labeled as cyan, orange, and green, respectively.

(IL-1RAcPb-ΔC) (Figure 2B). Correspondingly, the C-terminal tail of IL-1RAcPb was added to the C-terminus of IL-1RAcP in another clone (IL-1RAcP + bC) (Figure 2B). In parallel, we also constructed an IL-1RAcP clone with the absence of its own C-terminal tail (IL-1RAcP-ΔC) (Figure 2B). We examined the abilities of these IL-1RAcPb or IL-1RAcP mutants in mediating NF-κB activation after expressing them in HEK293T-IL-1RAcP-KO cells we previously reported by dual-luciferase reporter assay (Ge et al., 2019). After the transient expression of the wild-type IL-1RAcP, the HEK293T-IL-1RAcP-KO cells responded well to IL-1β treatment by showing detectable NF-κB activation (Figure 2B). Consistent with previous reports (Huang et al., 2011; Smith et al., 2009), wild-type IL-1RAcPb was not able to stimulate the NF-κB activity upon IL-1β treatment (Figure 2B). After deleting the C-terminal tail, the IL-1RAcPb-ΔC still could not gain the signaling function, and adding this long tail to the C-terminus of IL-1RAcP (IL-1RAcP + bC) also did not significantly inhibit its signaling function (Figure 2B). Likewise, the signaling function of IL-1RAcP-ΔC with its own short C-terminal tail deleted was also not significantly affected (Figure 2B). All these results indicate that neither the long C-terminal tail of IL-1RAcPb nor the shorter one of IL-1RAcP significantly affect the ability of IL-1RAcP in mediating NF-κB activation after IL-1β treatment. This also led us to assume that the inability of IL-1RAcPb in mediating NF-κB activation like IL-1RAcP is rooted in its variant TIR domain, not the C-terminal tail.

αC and αD of the TIR domain as the key regions affecting IL-1RAcP signaling

Sequence alignment showed that within the IL-1RAcP and IL-1RAcPb TIR domains, the N-terminal fragment and three classic sequence motifs (box1, box2, and box3) (Bowie and O'Neill, 2000) are conserved, whereas other regions in the TIR domain share only 35% sequence identity (Figure 3A). Currently, we do not have the structure of IL-1RAcP-TIR for direct comparison with that of IL-1RAcPb. However, the above structural

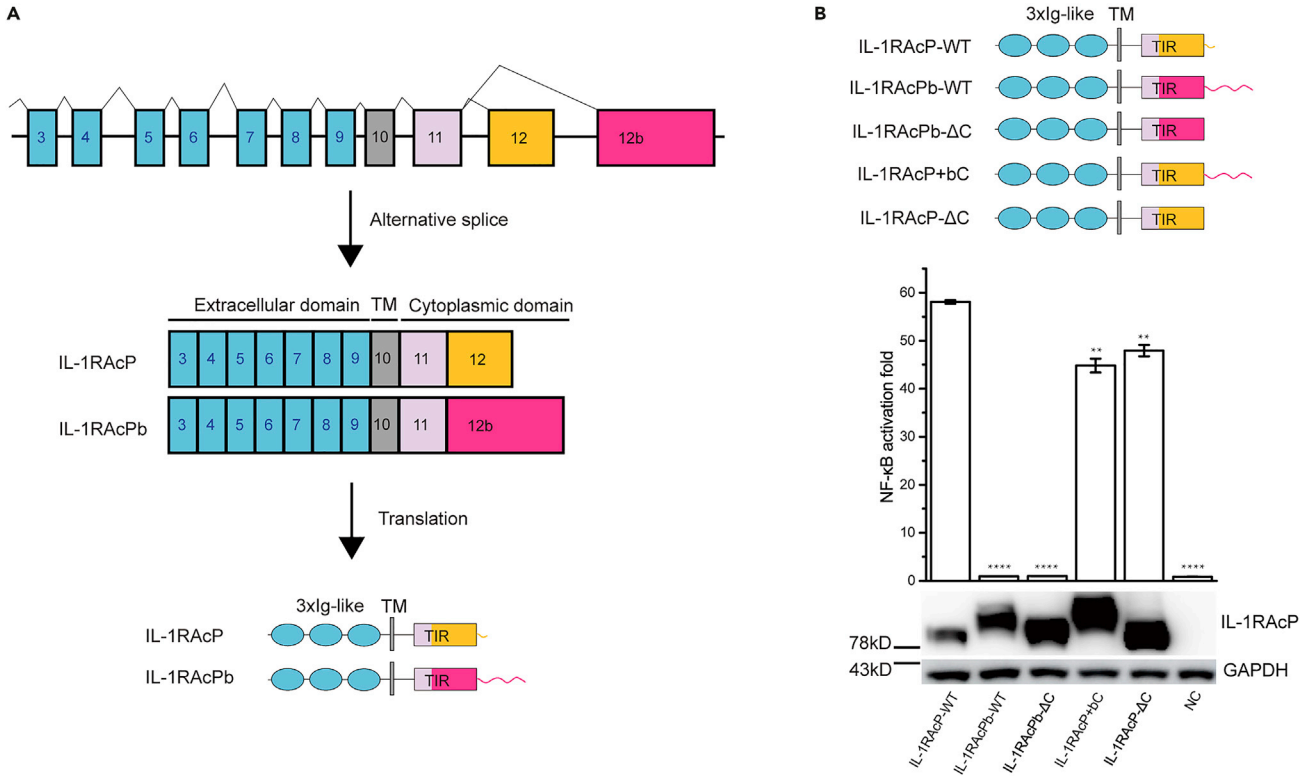

Figure 2. Genomic organization, protein architecture of IL-1RAcP isoforms, and measurement of effects of their C-terminal tail mutants on NF-κB activation signal

(A) A schematic representation of intron-exon map of human IL-1RAcP locus, alternative splicing, and subsequent translation that leads to the production of protein isoforms. Exons (3–12) encode the mature IL-1RAcP proteins, and differentiated utilization of exon 12 results in two different isoforms, which are distinguished in their TIR domains and C-terminal tails.

(B) Detection of the effects of IL-1RAcP and IL-1RAcPb C-terminal tails on NF-κB signaling. Each of IL-1RAcP-ΔC, IL-1RAcP + bC, IL-1RAcPb-ΔC mutants, IL-1RAcP-WT, IL-1RAcPb-WT, or empty constructs was co-transfected with luciferase reporter genes into 293T-IL-1RAcP-KO cells (with endogenous expression of IL-1RI). Then, cells were incubated with titrated concentrations of 5 nM IL-1β for 7 h prior to cell lysis. Finally, the NF-κB activity was measured by dual-luciferase reporter assay. All values represent means ± SD (n = 3). Significant differences between IL-1RAcP-WT group and the other groups were established by *Student's* t test. **p < 0.01, ****p < 0.0001. The protein levels of various IL-1RAcP were measured by Western blot analysis with the whole-cell lysate. The experiments were performed independently at least three times.

comparisons and analyses of IL-1R and TLR TIR domains clearly indicated that the αC and αD regions are variable and play important roles in the functional discrepancies between IL-1RAcP and IL-1RAcPb.

To explore the key segments for signal transduction discrepancy between IL-1RAcP and IL-1RAcPb, we constructed two IL-1RAcP mutants, in which the segments corresponding to αC and αD regions were replaced by the equivalents from IL-1RAcPb. Several similar substitutions were also made in other regions that were structurally similar but sequentially different from eliminating their possible influence on signaling function. These mutants were termed IL-1RAcP-b-swap1 to IL-1RAcP-b-swap9 (Figure 3A). The boundaries of these segments were chosen by considering sequence alignment and secondary structures derived from the crystal structure of IL-1RAcPb-TIR (Figures 3A and 3B). The swapped segments in IL-1RAcP-b-swap1, IL-1RAcP-b-swap4, IL-1RAcP-b-swap6, and IL-1RAcP-b-swap9 approximately correspond to αB, αC, αD, and αE, respectively. IL-1RAcP-b-swap2, IL-1RAcP-b-swap5, and IL-1RAcP-b-swap7 have replacements around βC, βD, and βE. The remaining two mutants (IL-1RAcP-b-swap3 and IL-1RAcP-b-swap8) mainly correspond to connecting loops. We first checked if these segment replacements affected protein expression in 293T-IL-1RAcP-KO cells. Western blot analysis showed that IL-1RAcP-b-swap5 and IL-1RAcP-b-swap7 showed poor expression, whereas wild-type IL-1RAcP and other mutants showed normal expression (Figure 3C). The 293T-IL-1RAcP-KO cells expressing these IL-1RAcP mutants were treated by IL-1β and assessed by the NF-κB dual-luciferase reporter assay. It was shown that IL-1RAcP-b-swap4, IL-1RAcP-b-swap5, IL-1RAcP-b-swap6, and IL-1RAcP-b-swap7 substantially or even completely lost the function of

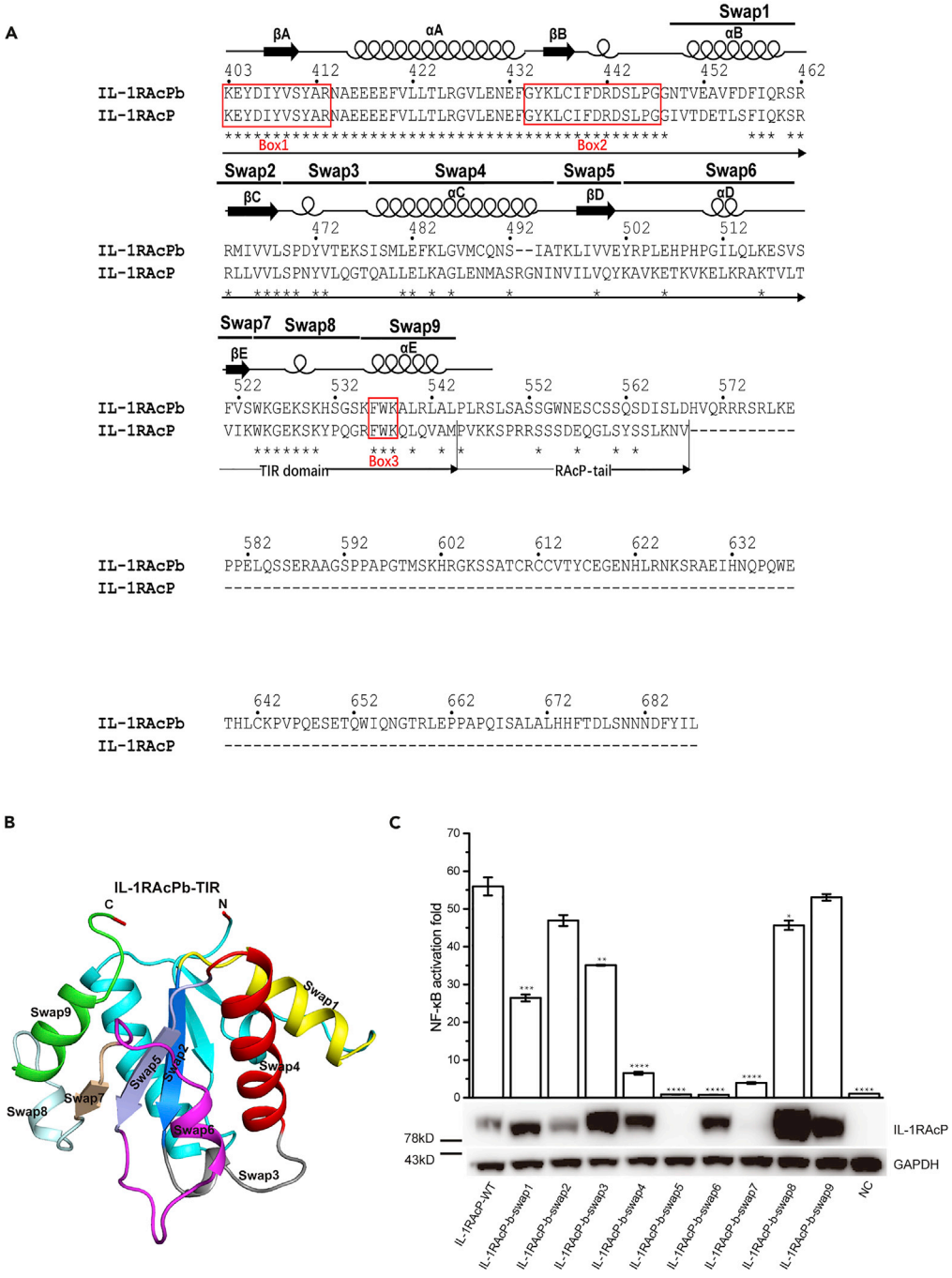

Figure 3. Sequence alignment of IL-1RAcP and IL-1RAcPb, division of swap regions of their TIR domains, and measurement of the effects of a series of IL-1RAcP swapping mutants on NF-κB activation signal

(A) Alignment of C termini of IL-1RAcP and IL-1RAcPb isoforms. Stars (*) indicate conserved residues between IL-1RAcP and IL-1RAcPb. Specific structural or signaling-associated motifs are indicated.

(B) Division of Swap regions in IL-1RAcPb-TIR based on sequence alignment and structural analysis. αB to αE of IL-1RAcPb-TIR are marked as Swap1 to Swap9 successively, and labeled by distinct colors. The Swap regions of IL-1RAcP-TIR and IL-1RAcPb-TIR are also shown in (A).

(C) Detecting the effects of a series of IL-1RAcP swapping mutants on NF-κB signaling. A series of IL-1RAcP mutants with swapped sequence (from Swap1 to Swap9) stemming from the corresponding regions of IL-1RAcPb were constructed. Each of these mutants, IL-1RAcP-WT or empty constructs was co-transfected with luciferase reporter genes into

Figure 3. *Continued*

293T-IL-1RAcP-KO cells. Subsequently, cells were stimulated by titrated concentrations of 5nM IL-1β for 7 h prior to cell lysis. The NF-κB activity was then measured. Data are shown as mean ± SD (n = 3). Significant differences between IL-1RAcP-WT group and the other groups were established by *Student's* t test. *p < 0.1, **p < 0.01, ***p < 0.001, ****p < 0.0001. The protein levels of various IL-1RAcP were measured by Western blot analysis with the whole-cell lysate. The experiments were performed independently at least three times.

mediating the activation of NF-κB signaling pathway (Figure 3C). The signaling function of IL-1RAcP-b-swap1 and IL-1RAcP-b-swap3 was partially affected, and that of IL-1RAcP-b-swap2, IL-1RAcP-b-swap8, and IL-1RAcP-b-swap9 was hardly impacted (Figure 3C). These results collectively indicate that failure of IL-1RAcP-b-swap5 and IL-1RAcP-b-swap7 to mediate NF-κB activation may be attributed to their inability of effective expression, and the swap1, swap3, swap4, and swap6 regions all are involved in the signaling function of the IL-1RAcP. Notably, nearly inactive IL-1RAcP-b-swap4 and IL-1RAcP-b-swap6 strongly suggest that αC and αD are the key determining regions of the IL-1RAcP signaling function. This conclusion is also consistent with crystal structure comparisons showing that the αC and αD are the most structurally variable regions in the TIR domain (Figure 1).

Important sites in the IL-1RAcP TIR domain affecting signaling

We also sought to pinpoint amino acid residues in the IL-1RAcP that are important for activating signaling. Based on sequence alignment, a series of single-site IL-1RAcP mutants were generated by changing the amino acid residues of IL-1RAcP-TIR individually to those of IL-1RAcPb-TIR, followed by the NF-κB dual-luciferase reporter assay (Figures 4A and S4A). We generated a total of thirty-eight IL-1RAcP mutants with single-site amino acid residue change in the swap4, swap5, swap6, and swap7 regions (Figure 4A). Among them, ten mutations including A485L, M490Q, A491N, I494A, V496K, Y501E, K502Y, V504P, E511G, and L519V significantly impaired the ability of IL-1RAcP in activating the NF-κB triggered by IL-1β (Figures 4A and 4B). And the Western blot experiment displayed that only IL-1RAcP mutants harboring V496K or Y501E mutation were not expressed normally (Figures 4A and 4B). For the remaining eight mutants that affecting the signaling, A485L, M490Q, A491N, and I494A are in the swap4 region around the αC, while K502Y, V504P, E511G, and L519V are in the swap6 region around the αD (Figure 4B). We also generated a total of fourteen IL-1RAcP mutants with single-site amino acid residue change in the swap1 and swap3 regions (Figure S4A). The luciferase assay results show there are no mutations that have a significant effect on the NF-κB activation. In addition, we noticed that IL-1RAcP TIR domain has a short insertion of -RG- at the C-terminus of the αC compared with that of IL-1RAcPb. The IL-1RAcP-ΔRG mutant with -RG- deletion failed to transduce IL-1β signal (Figure S4B). We also generated IL-1RAcP-RG-AG and IL-1RAcP-RG-EG mutants by changing the basic arginine to alanine or acidic glutamate, and these two IL-1RAcP mutants still transduced the IL-1β signal as well as the wild-type protein (Figure S4B). These results indicated that the glycine at the C-terminus of the αC plays a role in IL-1RAcP-mediated signaling (Figure 3A). Finally, after mapping these important sites for signaling on the surface of the IL-1RAcPb crystal structure, two separate patches could be defined with the Patch 1 consisting of Q490, N491, A494, and V519 and the Patch 2 consisting of Y502 and P504 (Figure 5).

IL-1RAcPb mutants partially mediating NF-κB activation

We have shown that swapping the regions around the αC and αD (swap4 and swap6) in the TIR domain of the IL-1RAcP inactivated the signaling function (Figure 3C). An interesting question emerged that if swapping in the same regions could enable the IL-1RAcPb to gain the signaling function. Therefore, we constructed two IL-1RAcPb mutants containing swap4 and swap6 in the TIR domain, but with the presence or absence of the long C-terminal tail after the TIR domain. These two mutants were IL-1RAcPb-RAcP-Swap4+Swap6-568 (Swap46-568 for short, in which the C-terminus was at the 568 position without the long C-terminal tail) and IL-1RAcPb-RAcP-Swap4+Swap6-end (Swap46-end, in which the C-terminal long tail was retained). Unfortunately, the expression of these two mutants in 293T-IL-1RAcP-KO cells was significantly reduced (Figure S5). And the dual-luciferase detection after IL-1β treatment consistently did not show NF-κB activation signal (Figure S5). We also tested adding the swap5 or swap7, resulting in four more IL-1RAcPb mutants including Swap456-568, Swap456-end, Swap467-568, and Swap467-end. There was still no improvement of the expression of these mutants and no obvious NF-κB activation signal after IL-1β treatment (Figure S5). Finally, after swapping the four regions (4–7) together, IL-1RAcPb mutants Swap4567-568 and Swap4567-end could partially mediate NF-κB activation, and the expression of these two mutants was also stronger than other IL-1RAcPb mutants (Figure 6). We also tried to see if important

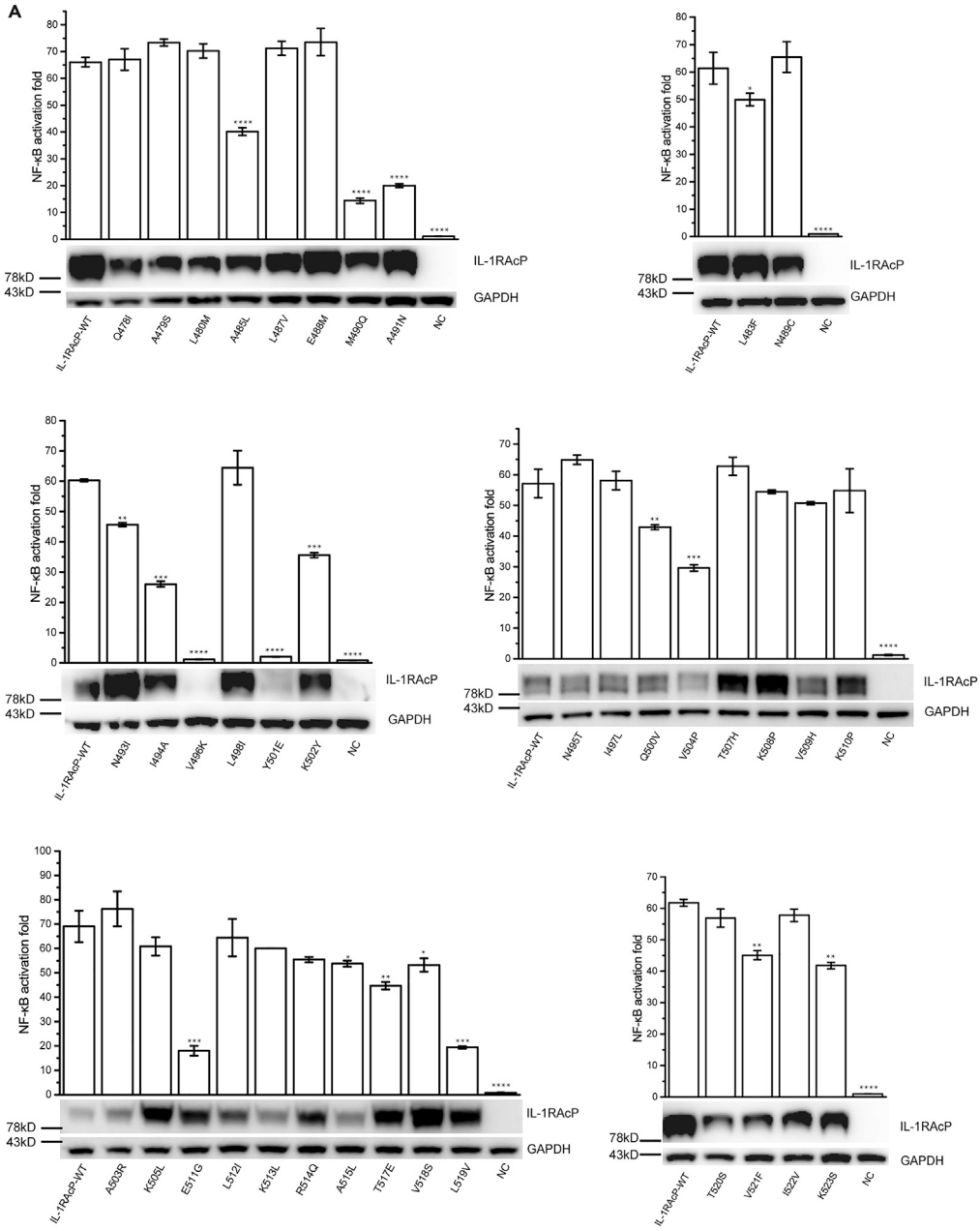

B

Summary of mutation sites in the IL-1RAcP TIR domain that significantly impaired the NF-κB activation

Regions / Item	Swap4 (αC)	Swap5 (βD)	Swap6 (αD)	Swap7 (βE)
Important sites in IL-1RAcP-TIR	485, 490, 491, 494	496※ 501※	502, 504 511, 519	- -

※indicates failure to express the corresponding site-directed mutant protein.

Figure 4. Measurement of effects of IL-1RAcP single-site mutations in Swap4/Swap5/Swap6/Swap7 regions of its TIR domain on NF-κB activation signal

(A and B) (A) A series of IL-1RAcP single-site mutants with swapped amino acid residues in Swap4/Swap5/Swap6/Swap7 regions of the TIR domain stemming from the corresponding sites of IL-1RAcPb were generated. Each of these mutants, IL-1RAcP-WT or empty constructs was co-transfected with luciferase reporter genes into 293T-IL-1RAcP-KO cells. Then, cells were incubated with titrated concentrations of 5 nM IL-1β for 7 h prior to cell lysis. Finally, the NF-κB activity was measured. All values represent means ± SD (n = 3). Significant differences between IL-1RAcP-WT group and the other groups were established by *Student's* t test. *p < 0.1, **p < 0.01, ***p < 0.001, ****p < 0.0001. The protein levels of various IL-1RAcP were measured by Western blot analysis with the whole-cell lysate. The experiments were performed independently at least three times. The mutation sites in IL-1RAcP TIR domain that significantly impaired the NF-κB activation are listed in (B).

single-site mutations could make the IL-1RAcPb to gain the function. However, all IL-1RAcPb mutants harboring combination of these single-site mutations in the TIR domain lost the expression and also did not show NF-κB activation signal (Figure S5). These results collectively indicated again that the region containing swap4 to swap7 is important for determining the functional discrepancy between IL-1RAcP and IL-1RAcPb to mediate IL-1 signaling, although currently we could not locate important single sites as in the IL-1RAcP.

DISCUSSION

The TIR domain is widely distributed in animal, plant, and bacterial proteins involved in innate immunity pathways and associated processes (Nimma et al., 2017; Toshchakov and Neuwald, 2020). It was originally defined to describe the cytoplasmic part of the TLRs and IL-1Rs (Gay and Keith, 1991). In mammals, the TIR domains are found in the intracellular part of TLRs and IL-1Rs, and also in their downstream adaptor proteins. Here, we report crystal structures of four IL-1R TIR domains from IL-1RAcPb (a splice isoform of co-receptor IL-1RAcP), IL-18Rβ and IL-1RAPL2, as well as the zebrafish SIGIRR. As a shared co-receptor, IL-1RAcP is critical in mediating the activities of several different IL-1 cytokines by forming signaling ternary complexes with cytokine and cytokine-binding primary receptor (Dinarello, 2009; Garlanda et al., 2013; Sims and Smith, 2010). Of note, IL-1RAcPb is unable to mediate NF-κB signaling triggered by IL-1 cytokines as IL-1RAcP due to the different cytoplasmic TIR-containing part caused by alternative splicing (Smith et al., 2009). Taking advantage of the IL-1RAcP/IL-1RAcPb pair and using mutagenesis (segment swapping and single-site mutation) and cell-based assays, we revealed that functional discrepancies between IL-1RAcP and IL-1RAcPb are determined by the variant TIR domain, not other regions in the cytoplasmic part. We also showed that the TIR αC- and αD-containing segments and several key sites in them are critical for the signaling activity of IL-1RAcP, which is supported by structural comparisons showing that the αC- and αD-containing segments are the most structurally variable among different IL-1R TIR domains.

Before this study, IL-1RAPL1 TIR domain is the only one in the IL-1R family whose crystal structure was determined (Khan et al., 2004). Here, we reported four more IL-1R TIR domain structures, including IL-1RAcPb, IL-18Rβ, IL-1RAPL2, and the zebrafish SIGIRR. IL-1RAcPb is a splice isoform of IL-1RAcP, which is a shared co-receptor for the signaling of six different agonists. In contrast, IL-18Rβ is a co-receptor only utilized by IL-18 for signaling (Garlanda et al., 2013). Although we do not have the structure of the IL-1RAcP TIR domain, structural comparisons showed that the IL-18Rβ TIR domain is distinct from other IL-1R TIR domains in the orientation of the αD helix, indicating that the αD may be involved in the specific TIR:TIR interaction between IL-18Rα and IL-18Rβ. Previously, there were also several reports about the mutagenesis of IL-1RI and IL-1RAcP TIR domain, trying to elucidate its ability in mediating the signaling. Alanine scanning of the boxes 1, 2, and 3 in the human IL-1RI TIR domain showed that boxes 1 and 2 are important for signaling, whereas mutagenesis in the box 3 motif did not affect the signal transduction (Slack et al., 2000). Modeling of the mouse IL-1RI TIR, site-directed mutagenesis, and NF-κB luciferase assay collectively showed that the αC′ helix (Q469-E473) may participate in the homotypic interactions with the TIR domains of IL-1RAcP and MyD88 (Radons et al., 2015). In contrast to the conclusions from the studies of the IL-1RI TIR domain, it was shown that the box 3 motif of the mouse IL-1RAcP TIR is important for the IL-1-dependent activation of NF-κB (Radons et al., 2002). And the K527-P534 segment is critical for the recruitment of MyD88 (Radons et al., 2003). Although we used similar mutagenesis and luciferase assay methods in this study, we took advantage of the IL-1RAcP/IL-1RAcPb pair and relevant structural information obtained from several crystal structures of IL-1R TIR domains (especially the IL-1RAcPb-TIR) that we determinated. By using segment swapping and then single-site mutagenesis in the IL-1RAcP TIR domain, we showed the importance of the αC and αD helices and eight sites (A485, M490, A491, I494, K502, V504,

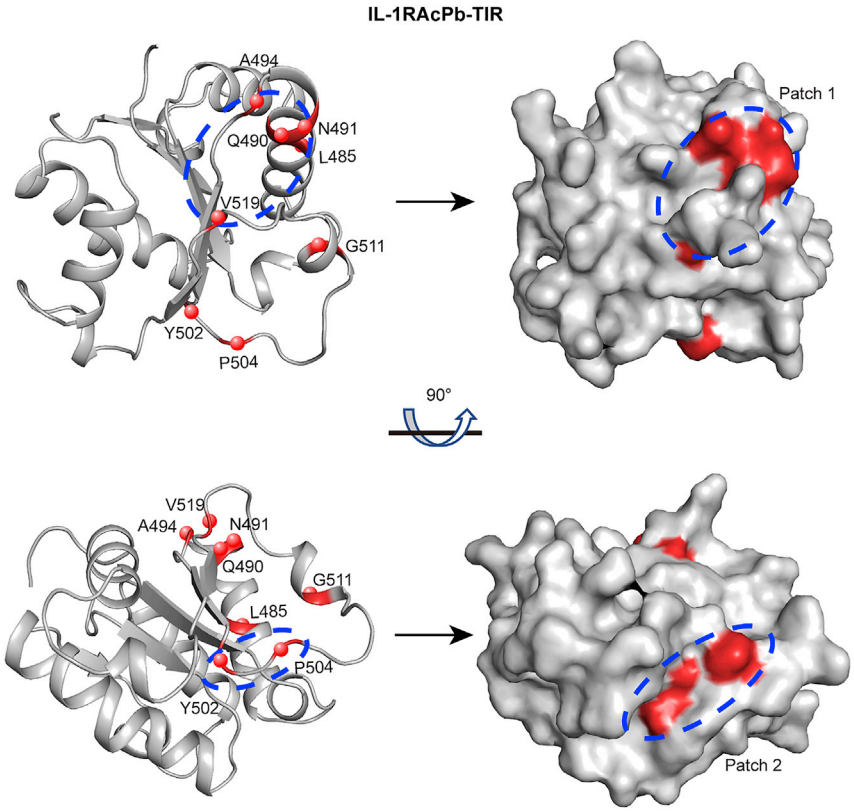

Figure 5. The distribution of significant signaling-affecting sites of IL-1RAcP TIR mapped on IL-1RAcPb TIR structure surface

The residues in IL-1RAcPb-TIR corresponding to the significant signaling-affecting ones of IL-1RAcP-TIR are shown as red spheres with positions labeled. These residues are mainly distributed on two patches of the molecular surface of IL-1RAcPb-TIR: Patch 1 and Patch 2.

E511, and L519) on them in mediating signaling. Comparing the three-dimensional structure of IL-1RAcP-TIR predicted by AlphaFold2 with that of IL-1RAcPb-TIR, we found that there are obvious structural differences in the αC and αD regions, which further confirms the critical roles of these two regions for signaling (Callaway, 2021) (Figure S6).

TIR domains function as protein scaffolds mostly through self- and homotypic-association with other TIR domains. Structures of plant and bacterial TIR domains have revealed TIR:TIR interactions that are functionally relevant, which involve highly conserved interfaces, respectively (Alaidarous et al., 2014; Bernoux et al., 2011; Chan et al., 2009, 2010; Kaplan-Turkoz et al., 2013; Ma et al., 2020; Nimma et al., 2017; Snyder et al., 2014; Ve et al., 2015; Williams et al., 2014; Zhang et al., 2017). However, no common TIR:TIR interaction interfaces have been observed in structures of mammalian TIR domains. Various methods, such as structure analysis, mutagenesis, and molecular docking, have been used in a number of studies, proposing different models of mammalian TIR domain assembly with some common trends (Bovijn et al., 2012, 2013; Clabbers et al., 2021; Enokizono et al., 2013; Guven-Maiorov et al., 2015; Khan et al., 2004; Nunez Miguel et al., 2007; Ohnishi et al., 2009; Tao et al., 2002; Toshchakov et al., 2011; Ve et al., 2017; Vyncke et al., 2016). For example, crystal structures of TLR (TLR1-TIR, TLR2-TIR, TLR6-TIR, and TLR10-TIR), IL-1R (IL-1RAPL1-TIR), and adaptors (MAL-TIR, SARM1-TIR, and BCAP-TIR) all contain a similar TIR:TIR interface (defined as BCD interface), consisting of the αC regions and either the αB/BB loop or the αD regions, or both (Halabi et al., 2017; Horsefield et al., 2019; Jang and Park, 2014; Khan et al., 2004; Lin et al., 2012; Nimma et al., 2021; Nyman et al., 2008; Xu et al., 2000) (Figures 7 and S7). Many loss-of-function mutations in TLR4 are located at the BCD interface (Bovijn et al., 2012, 2013; Guven-Maiorov et al., 2015; Nunez Miguel et al., 2007). Besides, a naturally occurring mutation P712H resulting in the no-response of TLR4 to LPS is also located in the BB loop (Poltorak et al., 1998). Other receptor or adaptor TIR domains with such mutation also lose the

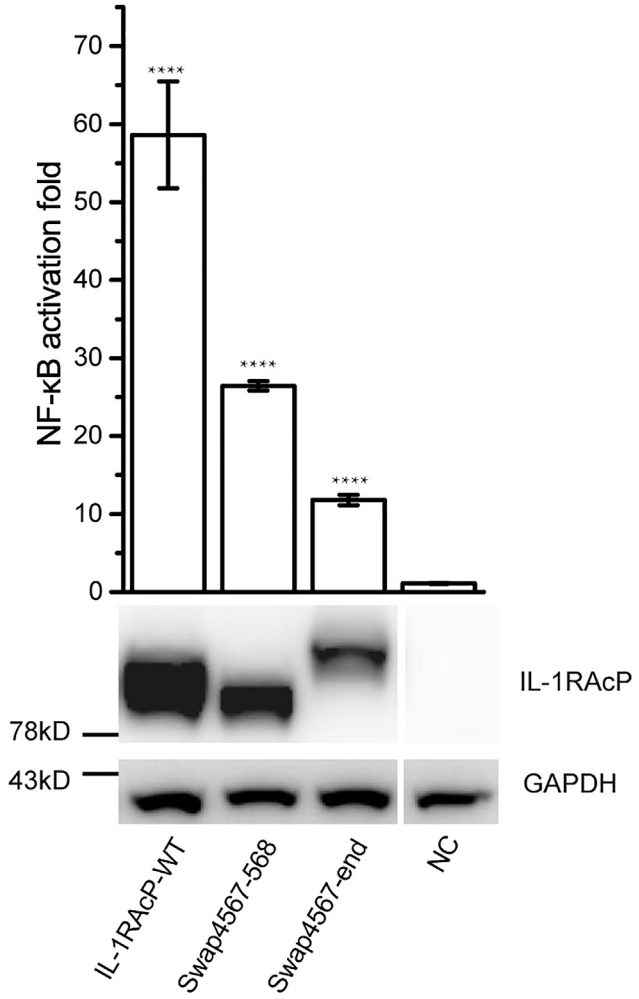

Figure 6. Specific IL-1RAcPb mutants gaining the NF-κB signaling function

Each of Swap4567-568, Swap4567-end mutants, IL-1RAcP-WT, or empty constructs was co-transfected with luciferase reporter genes into 293T-IL-1RAcP-KO cells. Then cells were stimulated with titrated concentrations of 5nM IL-1β for 7 h prior to cell lysis. Finally, the NF-κB activity was measured. Data are shown as means ± SD (n = 3). Significant differences between negative control (NC) group and the other groups were established by *Student's* t test. ****$p < 0.0001$. The protein levels of various IL-1RAcP were measured by Western blot analysis with the whole-cell lysate. The experiments were performed independently at least three times.

signaling function (Nimma et al., 2017). Mutations of MAL-TIR in the interface comprising the αC and αD regions prevent both MAL-TIR and MyD88-TIR binding (Lin et al., 2012; Valkov et al., 2011). These functional results suggest that the BCD interface could be physiologically relevant. Besides, TIR:TIR interfaces observed in several mammalian TIR domain crystal structures coincide with transient complexes in solution (Bovijn et al., 2012; Lin et al., 2012; Nunez Miguel et al., 2007; Valkov et al., 2011).

Generally, it is challenging to reconstitute stable mammalian TIR domain complexes *in vitro* for structural studies (Nimma et al., 2017), probably due to the weak TIR:TIR interactions and/or the tendency to aggregate. Fortunately, in 2017, Ve et al. reported that the MAL-TIR spontaneously and reversibly forms filaments *in vitro* and induces formation of MyD88-TIR crystalline higher-order assemblies (Ve et al., 2017). Besides, they also successfully reconstituted co-assemblies of TLR4-TIR and MAL-TIR domains in this paper (Ve et al., 2017). The cryo-EM structure of MAL-TIR protofilament, as well as the MicroED and serial femtosecond crystallography (SFX) structures of the MyD88-TIR assembly all revealed an analogous two-stranded higher-order assembly arrangement of TIR domain subunits (Clabbers et al., 2021; Ve et al., 2017). There are two major types of asymmetric interactions between these subunits, including a BB

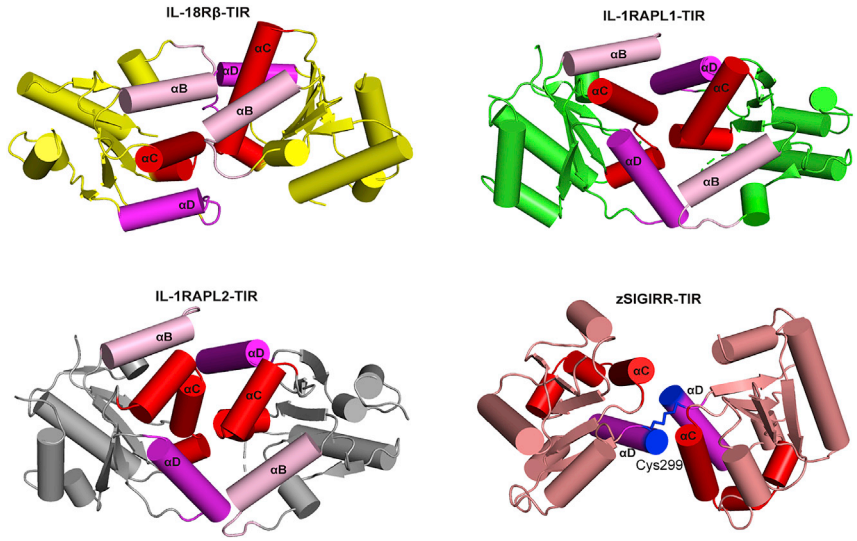

Figure 7. BCD interaction interfaces in IL-1R TIR crystal structures

Shown are the cartoon representation of homo-dimer from the crystal structures of IL-18Rβ-TIR (yellow), IL-1RAPL1-TIR (PDB ID: 1T3G, green), IL-1RAPL2-TIR (gray70), and zSIGIRR-TIR (salmon). αB/BB loop (light pink), αC (red), and αD (magenta) regions, or αC and either of the other two regions constitute BCD interaction interfaces. The disulfide bonds (blue) were observed in BCD interfaces of zSIGIRR-TIR.

loop-mediated head-to-tail "BE" intrastrand interaction, involving the region around the BB loop of one subunit and the EE surface (the βD and βE strands and the αE helix) of the next subunit; and an interstrand interaction consisting of the BC surface (αB and αC helices) from one subunit and the CD surface (αD helix and CD loop) from another (BCD interface). Through structure-guided mutagenesis, *in vivo* interaction assays, and cell-based signaling assays, they demonstrated that the interactions defined within the MAL-TIR filament and the MyD88-TIR assembly crystals represent a template for a conserved mode of TIR-domain interaction involved in TLR and IL-1R signaling (Clabbers et al., 2021; Ve et al., 2017).

In this study, inspecting the structures of the IL-1R TIR domains with the help of PISA server also revealed a similar BCD interface in IL-18Rβ-TIR, IL-1RAPL2-TIR, and zSIGIRR-TIR, but not in IL-1RAcPb-TIR crystal packing (Krissinel and Henrick, 2007) (Figure 7 and Tables S2–S5). Specifically, the interface of IL-18Rβ-TIR buries 8.7%–8.9% (667–678 Å^2) of the total surface area per monomer in the structure and is composed of interactions between residues located in the αB/BB loop, αC, and αD/DD loop regions (Figure 7 and Table S2). With slight difference in buried surface area, the BCD interfaces of IL-1RAPL2-TIR [13.6%–13.7% (1,196–1,197 Å^2)] and IL-1RAPL1-TIR (PDB ID: 1T3G) [12.2%–12.3% (1,041–1,061 Å^2)] all consist of interactions between residues mainly from αB/BB loop, αC, and αD regions of each molecule (Figure 7 and Tables S3 and S4). Besides, the interface of zSIGIRR-TIR buries 4.8% (378–382 Å^2) of the total surface area per monomer and comprises interactions between residues located in the αC, CD loop, and αD regions (Figure 7 and Table S5). There are several hydrogen bonds and less salt bridges in these BCD interfaces (Tables S2–S5). In addition, a disulfide bond between the two Cys299 in the αD region of the two chains was noted, which is important for zSIGIRR-TIR dimerization as the mutant zSIGIRR-C299S-TIR exists as monomer in solution (Figure 7 and Table S5). Our structural analysis results further support the BCD interface as a common interaction interface for TIR domains in the TLR/IL-1R family. Moreover, the dual-luciferase reporter assay also showed that αB, αC, and αD regions (especially the structurally variable αC and αD) are significantly important for IL-1RAcP signaling function. In light of these crystal structural analyses, functional assays, and previous studies, we propose that IL-1RAcP requires homo-dimerization/-oligomerization in its mediation of NF-κB signaling (Figure S8); and the alternation of αB, αC, and αD in IL-1RAcPb-TIR impairs or even destroys its self-association, leading to the reduction or loss of NF-κB signaling function of IL-1RAcPb.

Interestingly, in 2017, Essuman et al. demonstrated for the first time that the TIR domain of the adaptor protein SARM1 possesses NAD^+ enzymatic function, which plays an important role in the neuron axon degeneration process, and further identified E642 as the catalytic site (Figure S9) (Essuman et al., 2017). Subsequently, multiple TIR domains from archaea/bacteria and plants have also been shown to possess

NAD^+ enzymatic function, which plays a key role in bacterial immune evasion and plant cell death pathways (Essuman et al., 2018; Horsefield et al., 2019; Ma et al., 2020; Wan et al., 2019). In this study, alignment of the crystal structures of TIR domains from TLRs, IL-1Rs, and adaptor proteins with that of SARM1-TIR showed that only IL-1RAcPb-TIR and IL-18Rβ-TIR are highly structurally similar to SARM1-TIR with a conserved catalytic site (Horsefield et al., 2019) (Figure S9). However, merely, the potential catalytic site of IL-18Rβ-TIR is exposed to the surface. In addition, the three-dimensional structure of IL-1RAcP-TIR predicted by AlphaFold2 is also analogous to that of SARM1-TIR with the conserved catalytic site (Figure S9). Therefore, it will be very interesting and important to further explore whether the TIR domains of the co-receptor IL-1RAcP and IL-18Rβ possess NAD^+ enzymatic activity, how this catalytic function relates to the signaling functions, and whether it is related to the selection of co-receptors (IL-1RAcP and IL-18Rβ).

Limitations of the study

This study promotes additional information for our understanding of the IL-1R family, especially the IL-1RAcP signal transduction mechanism. But there are still some limitations. For instance, the structure of IL-1RAcP-TIR was not successfully determined, which to some extent hindered our understanding of its functional mechanism. Here, we only utilize IL-1RAcPb as the template to perform mutation experiments between IL-1RAcP-TIR and IL-1RAcPb-TIR, thus some important functional positions might not be identified. Additionally, in this field, there are still some key issues to be addressed. For example, there are both similarities and differences of functions performed by IL-1R family members, and the structural and functional commonalities or specificities between their corresponding TIR domains have not yet been fully understood. Moreover, how the IL-1R TIR domains cooperate with each other to transmit signaling to downstream adaptors still needs further elucidation. Therefore, more structure determination and corresponding functional analysis of IL-1R TIR domains in the future are of vital importance to better understand the physiological functions of this family.

STAR★METHODS

Detailed methods are provided in the online version of this paper and include the following:

- KEY RESOURCES TABLE
- RESOURCE AVAILABILITY
  - Lead contact
  - Materials availability
  - Data and code availability
- EXPERIMENTAL MODEL AND SUBJECT DETAILS
- METHOD DETAILS
  - Plasmid construction
  - Protein expression and purification
  - Crystallization and diffraction data collection
  - Structure determination and refinement
  - Dual-luciferase report assays
  - Western blot
- QUANTIFICATION AND STATISTICAL ANALYSIS

SUPPLEMENTAL INFORMATION

Supplemental information can be found online at https://doi.org/10.1016/j.isci.2022.104508.

ACKNOWLEDGMENTS

We thank the SSRF BL17U beam line for data collection and processing. We thank at the X-ray crystallography platform of the Tsinghua University Technology Center for Protein Research for providing the facility support. This work was supported by funds from China Postdoctoral Science Foundation (2020M670295).

AUTHOR CONTRIBUTIONS

J.Z. carried out plasmid construction, protein expression, purification, crystallization, diffraction data collection, structure determination, dual-luciferase reporter assay, and Western blot experiments. X.W. and Y.X. helped in structure determination. Y.R. was involved in some plasmid's construction. The

293T-IL-1RAcP-KO cell line was generated by J.G. in a previous study. X.W. conceived and directed the study. J.Z. analyzed the data and made the figures. J.Z. and X.W. wrote the manuscript.

DECLARATION OF INTERESTS

The authors declare no competing interests.

Received: August 2, 2021
Revised: May 2, 2022
Accepted: May 27, 2022
Published: July 15, 2022

REFERENCES

Afonine, P.V., Grosse-Kunstleve, R.W., Echols, N., Headd, J.J., Moriarty, N.W., Mustyakimov, M., Terwilliger, T.C., Urzhumtsev, A., Zwart, P.H., and Adams, P.D. (2012). Towards automated crystallographic structure refinement with phenix.refine. Acta Crystallogr. D Biol. Crystallogr. *68*, 352–367. https://doi.org/10.1107/s0907444912001308.

Alaidarous, M., Ve, T., Casey, L.W., Valkov, E., Ericsson, D.J., Ullah, M.O., Schembri, M.A., Mansell, A., Sweet, M.J., and Kobe, B. (2014). Mechanism of bacterial interference with TLR4 signaling by Brucella Toll/interleukin-1 receptor domain-containing protein TcpB. J. Biol. Chem. *289*, 654–668. https://doi.org/10.1074/jbc.m113.523274.

Bernoux, M., Ve, T., Williams, S., Warren, C., Hatters, D., Valkov, E., Zhang, X.X., Ellis, J.G., Kobe, B., and Dodds, P.N. (2011). Structural and functional analysis of a plant resistance protein TIR domain reveals interfaces for self-association, signaling, and autoregulation. Cell Host Microbe *9*, 200–211. https://doi.org/10.1016/j.chom.2011.02.009.

Boraschi, D., Italiani, P., Weil, S., and Martin, M.U. (2018). The family of the interleukin-1 receptors. Immunol. Rev. *281*, 197–232. https://doi.org/10.1111/imr.12606.

Boraschi, D., and Tagliabue, A. (2006). The interleukin-1 receptor family. Vitam. Horm. *74*, 229–254. https://doi.org/10.1016/S0083-6729(06)74009-2.

Bovijn, C., Desmet, A.S., Uyttendaele, I., Van Acker, T., Tavernier, J., and Peelman, F. (2013). Identification of binding sites for myeloid differentiation primary response gene 88 (MyD88) and Toll-like receptor 4 in MyD88 adapter-like (Mal). J. Biol. Chem. *288*, 12054–12066. https://doi.org/10.1074/jbc.m112.415810.

Bovijn, C., Ulrichts, P., De Smet, A.S., Catteeuw, D., Beyaert, R., Tavernier, J., and Peelman, F. (2012). Identification of interaction sites for dimerization and adapter recruitment in Toll/interleukin-1 receptor (TIR) domain of Toll-like receptor 4. J. Biol. Chem. *287*, 4088–4098. https://doi.org/10.1074/jbc.m111.282350.

Bowie, A., and O'Neill, L.A. (2000). The interleukin-1 receptor/Toll-like receptor superfamily: signal generators for pro-inflammatory interleukins and microbial products. J. Leukoc. Biol. *67*, 508–514. https://doi.org/10.1002/jlb.67.4.508.

Callaway, E. (2021). Deepmind's Ai predicts structures for a vast trove of proteins. Nature *595*, 635. https://doi.org/10.1038/d41586-021-02025-4.

Chan, S.L., Low, L.Y., Hsu, S., Li, S., Liu, T., Santelli, E., Le Negrate, G., Reed, J.C., Woods, V.L., and Pascual, J. (2009). Molecular mimicry in innate immunity. Crystal structure of a bacterial TIR domain. J. Biol. Chem. *284*, 21386–21392. https://doi.org/10.1074/jbc.c109.007591.

Chan, S.L., Mukasa, T., Santelli, E., Low, L.Y., and Pascual, J. (2010). The crystal structure of a TIR domain from Arabidopsis thaliana reveals a conserved helical region unique to plants. Protein Sci. *19*, 155–161. https://doi.org/10.1002/pro.275.

Clabbers, M.T.B., Holmes, S., Muusse, T.W., Vajjhala, P.R., Thygesen, S.J., Malde, A.K., Hunter, D.J.B., Croll, T.I., Flueckiger, L., Nanson, J.D., et al. (2021). MyD88 TIR domain higher-order assembly interactions revealed by microcrystal electron diffraction and serial femtosecond crystallography. Nat. Commun. *12*, 2578. https://doi.org/10.1038/s41467-021-22590-6.

Dinarello, C.A. (2009). Immunological and inflammatory functions of the interleukin-1 family. Annu. Rev. Immunol. *27*, 519–550. https://doi.org/10.1146/annurev.immunol.021908.132612.

Emsley, P., Lohkamp, B., Scott, W.G., and Cowtan, K. (2010). Features and development of coot. Acta Crystallogr. D Biol. Crystallogr. *66*, 486–501. https://doi.org/10.1107/s0907444910007493.

Enokizono, Y., Kumeta, H., Funami, K., Horiuchi, M., Sarmiento, J., Yamashita, K., Standley, D.M., Matsumoto, M., Seya, T., and Inagaki, F. (2013). Structures and interface mapping of the TIR domain-containing adaptor molecules involved in interferon signaling. Proc. Natl. Acad. Sci. U S A *110*, 19908–19913. https://doi.org/10.1073/pnas.1222811110.

Essuman, K., Summers, D.W., Sasaki, Y., Mao, X., DiAntonio, A., and Milbrandt, J. (2017). The SARM1 Toll/interleukin-1 receptor domain possesses intrinsic NAD(+) cleavage activity that promotes pathological axonal degeneration. Neuron *93*, 1334–1343.e5. https://doi.org/10.1016/j.neuron.2017.02.022.

Essuman, K., Summers, D.W., Sasaki, Y., Mao, X., Yim, A.K.Y., DiAntonio, A., and Milbrandt, J. (2018). TIR domain proteins are an ancient family of NAD(+)-Consuming enzymes. Curr. Biol. *28*, 421–430.e4. https://doi.org/10.1016/j.cub.2017.12.024.

Fields, J.K., Gunther, S., and Sundberg, E.J. (2019). Structural basis of IL-1 family cytokine signaling. Front. Immunol. *10*, 1412. https://doi.org/10.3389/fimmu.2019.01412.

Gabay, C., Lamacchia, C., and Palmer, G. (2010). IL-1 pathways in inflammation and human diseases. Nat. Rev. Rheumatol. *6*, 232–241. https://doi.org/10.1038/nrrheum.2010.4.

Garlanda, C., Dinarello, C.A., and Mantovani, A. (2013). The interleukin-1 family: back to the future. Immunity *39*, 1003–1018. https://doi.org/10.1016/j.immuni.2013.11.010.

Gay, N.J., and Keith, F.J. (1991). Drosophila Toll and IL-1 receptor. Nature *351*, 355–356. https://doi.org/10.1038/351355b0.

Ge, J., Remesh, S.G., Hammel, M., Pan, S., Mahan, A.D., Wang, S., and Wang, X. (2019). Functional relevance of interleukin-1 receptor inter-domain flexibility for cytokine binding and signaling. Structure *27*, 1296–1307.e5. https://doi.org/10.1016/j.str.2019.05.011.

Gosselin, D., Bellavance, M.A., and Rivest, S. (2013). IL-1RAcPb signaling regulates adaptive mechanisms in neurons that promote their long-term survival following excitotoxic insults. Front. Cell. Neurosci. *7*, 9. https://doi.org/10.3389/fncel.2013.00009.

Gunther, S., Deredge, D., Bowers, A.L., Luchini, A., Bonsor, D.A., Beadenkopf, R., Liotta, L., Wintrode, P.L., and Sundberg, E.J. (2017). IL-1 family cytokines use distinct molecular mechanisms to signal through their shared Co-receptor. Immunity *47*, 510–523.e4. https://doi.org/10.1016/j.immuni.2017.08.004.

Guven-Maiorov, E., Keskin, O., Gursoy, A., VanWaes, C., Chen, Z., Tsai, C.J., and Nussinov, R. (2015). The architecture of the TIR domain signalosome in the Toll-like receptor-4 signaling pathway. Sci. Rep. *5*, 13128. https://doi.org/10.1038/srep13128.

Halabi, S., Sekine, E., Verstak, B., Gay, N.J., and Moncrieffe, M.C. (2017). Structure of the Toll/interleukin-1 receptor (TIR) domain of the B-cell adaptor that links phosphoinositide metabolism with the negative regulation of the Toll-like receptor (TLR) signalosome. J. Biol. Chem. *292*, 652–660. https://doi.org/10.1074/jbc.m116.761528.

Holm, L. (2020). Using dali for protein structure comparison. Methods Mol. Biol. *2112*, 29–42. https://doi.org/10.1007/978-1-0716-0270-6_3.

Horsefield, S., Burdett, H., Zhang, X.X., Manik, M.K., Shi, Y., Chen, J., Qi, T.C., Gilley, J., Lai, J.S., Rank, M.X., et al. (2019). NAD $^+$ cleavage activity by animal and plant TIR domains in cell death pathways. Science *365*, 793–799. https://doi.org/10.1126/science.aax1911.

Huang, Y., Smith, D.E., Ibanez-Sandoval, O., Sims, J.E., and Friedman, W.J. (2011). Neuron-specific effects of interleukin-1 are mediated by a novel isoform of the IL-1 receptor accessory protein. J. Neurosci. *31*, 18048–18059. https://doi.org/10.1523/jneurosci.4067-11.2011.

Jang, T.H., and Park, H.H. (2014). Crystal structure of TIR domain of TLR6 reveals novel dimeric interface of TIR-TIR interaction for Toll-like receptor signaling pathway. J. Mol. Biol. *426*, 3305–3313. https://doi.org/10.1016/j.jmb.2014.07.024.

Janson, G., Zhang, C., Prado, M.G., and Paiardini, A. (2017). PyMod 2.0: improvements in protein sequence-structure analysis and homology modeling within PyMOL. Bioinformatics *33*, 444–446. https://doi.org/10.1093/bioinformatics/btw638.

Kaplan-Turkoz, B., Koelblen, T., Felix, C., Candusso, M.P., O'Callaghan, D., Vergunst, A.C., and Terradot, L. (2013). Structure of the Toll/interleukin 1 receptor (TIR) domain of the immunosuppressive Brucella effector BtpA/Btp1/TcpB. FEBS Lett. *587*, 3412–3416. https://doi.org/10.1016/j.febslet.2013.09.007.

Khan, J.A., Brint, E.K., O'Neill, L.A., and Tong, L. (2004). Crystal structure of the Toll/interleukin-1 receptor domain of human IL-1RAPL. J. Biol. Chem. *279*, 31664–31670. https://doi.org/10.1074/jbc.m403434200.

Krissinel, E., and Henrick, K. (2007). Inference of macromolecular assemblies from crystalline state. J. Mol. Biol. *372*, 774–797. https://doi.org/10.1016/j.jmb.2007.05.022.

Lin, Z., Lu, J., Zhou, W., and Shen, Y. (2012). Structural insights into TIR domain specificity of the bridging adaptor Mal in TLR4 signaling. PLoS One *7*, e34202. https://doi.org/10.1371/journal.pone.0034202.

Liu, X., Hammel, M., He, Y.F., Tainer, J.A., Jeng, U.S., Zhang, L.Q., Wang, S.Y., and Wang, X.Q. (2013). Structural insights into the interaction of IL-33 with its receptors. Proc. Natl. Acad. Sci. U S A *110*, 14918–14923. https://doi.org/10.1073/pnas.1308651110.

Ma, S.C., Lapin, D., Liu, L., Sun, Y., Song, W., Zhang, X.X., Logemann, E., Yu, D.L., Wang, J., Jirschitzka, J., et al. (2020). Direct pathogen-induced assembly of an NLR immune receptor complex to form a holoenzyme. Science *370*, eabe3069. https://doi.org/10.1126/science.abe3069.

McCoy, A.J., Grosse-Kunstleve, R.W., Adams, P.D., Winn, M.D., Storoni, L.C., and Read, R.J. (2007). Phaser crystallographic software. J. Appl. Crystallogr. *40*, 658–674. https://doi.org/10.1107/s0021889807021206.

Narayanan, K.B., and Park, H.H. (2015). Toll/interleukin-1 receptor (TIR) domain-mediated cellular signaling pathways. Apoptosis *20*, 196–209. https://doi.org/10.1007/s10495-014-1073-1.

Nguyen, L., Rothwell, N.J., Pinteaux, E., and Boutin, H. (2011). Contribution of interleukin-1 receptor accessory protein B to interleukin-1 actions in neuronal cells. Neurosignals *19*, 222–230. https://doi.org/10.1159/000330803.

Nimma, S., Gu, W., Maruta, N., Li, Y., Pan, M., Saikot, F.K., Lim, B.Y.J., McGuinness, H.Y., Zaoti, Z.F., Li, S., et al. (2021). Structural evolution of TIR-domain signalosomes. Front. Immunol. *12*, 784484. https://doi.org/10.3389/fimmu.2021.784484.

Nimma, S., Ve, T., Williams, S.J., and Kobe, B. (2017). Towards the structure of the TIR-domain signalosome. Curr. Opin. Struct. Biol. *43*, 122–130. https://doi.org/10.1016/j.sbi.2016.12.014.

Nunez Miguel, R., Wong, J., Westoll, J.F., Brooks, H.J., O'Neill, L.A., Gay, N.J., Bryant, C.E., and Monie, T.P. (2007). A dimer of the Toll-like receptor 4 cytoplasmic domain provides a specific scaffold for the recruitment of signalling adaptor proteins. PLoS One *2*, e788. https://doi.org/10.1371/journal.pone.0000788.

Nyman, T., Stenmark, P., Flodin, S., Johansson, I., Hammarström, M., and Nordlund, P. (2008). The crystal structure of the human Toll-like receptor 10 cytoplasmic domain reveals a putative signaling dimer. J. Biol. Chem. *283*, 11861–11865. https://doi.org/10.1074/jbc.c800001200.

Ohnishi, H., Tochio, H., Kato, Z., Orii, K.E., Li, A., Kimura, T., Hiroaki, H., Kondo, N., and Shirakawa, M. (2009). Structural basis for the multiple interactions of the MyD88 TIR domain in TLR4 signaling. Proc. Natl. Acad. Sci. U S A *106*, 10260–10265. https://doi.org/10.1073/pnas.0812956106.

Otwinowski, Z., and Minor, W. (1997). [20] Processing of X-ray diffraction data collected in oscillation mode. Methods Enzymol. *276*, 307–326. https://doi.org/10.1016/S0076-6879(97)76066-X.

Poltorak, A., He, X., Smirnova, I., Liu, M.Y., Van Huffel, C., Du, X., Birdwell, D., Alejos, E., Silva, M., Galanos, C., et al. (1998). Defective LPS signaling in C3H/HeJ and C57BL/10ScCr mice: mutations in Tlr4 gene. Science *282*, 2085–2088. https://doi.org/10.1126/science.282.5396.2085.

Prieto, G.A., Snigdha, S., Baglietto-Vargas, D., Smith, E.D., Berchtold, N.C., Tong, L., Ajami, D., LaFerla, F.M., Rebek, J., Jr., and Cotman, C.W. (2015). Synapse-specific IL-1 receptor subunit reconfiguration augments vulnerability to IL-1β in the aged hippocampus. Proc. Natl. Acad. Sci. U S A *112*, E5078–E5087. https://doi.org/10.1073/pnas.1514486112.

Radons, J., Dove, S., Neumann, D., Altmann, R., Botzki, A., Martin, M.U., and Falk, W. (2003). The interleukin 1 (IL-1) receptor accessory protein Toll/IL-1 receptor domain: analysis of putative interaction sites in vitro mutagenesis and molecular modeling. J. Biol. Chem. *278*, 49145–49153. https://doi.org/10.1074/jbc.m306077200.

Radons, J., Falk, W., and Dove, S. (2015). Identification of critical regions within the TIR domain of IL-1 receptor type I. Int. J. Biochem. Cell Biol. *68*, 15–20. https://doi.org/10.1016/j.biocel.2015.08.009.

Radons, J., Gabler, S., Wesche, H., Korherr, C., Hofmeister, R., and Falk, W. (2002). Identification of essential regions in the cytoplasmic tail of interleukin-1 receptor accessory protein critical for interleukin-1 signaling. J. Biol. Chem. *277*, 16456–16463. https://doi.org/10.1074/jbc.m201000200.

Schreuder, H., Tardif, C., Trump-Kallmeyer, S., Soffientini, A., Sarubbi, E., Akeson, A., Bowlin, T., Yanofsky, S., and Barrett, R.W. (1997). A new cytokine-receptor binding mode revealed by the crystal structure of the IL-1 receptor with an antagonist. Nature *386*, 194–200. https://doi.org/10.1038/386194a0.

Sims, J.E., and Smith, D.E. (2010). The IL-1 family: regulators of immunity. Nat. Rev. Immunol. *10*, 89–102. https://doi.org/10.1038/nri2691.

Slack, J.L., Schooley, K., Bonnert, T.P., Mitcham, J.L., Qwarnstrom, E.E., Sims, J.E., and Dower, S.K. (2000). Identification of two major sites in the type I interleukin-1 receptor cytoplasmic region responsible for coupling to pro-inflammatory signaling pathways. J. Biol. Chem. *275*, 4670–4678. https://doi.org/10.1074/jbc.275.7.4670.

Smith, D.E., Lipsky, B.P., Russell, C., Ketchem, R.R., Kirchner, J., Hensley, K., Huang, Y., Friedman, W.J., Boissonneault, V., Plante, M.M., et al. (2009). A central nervous system-restricted isoform of the interleukin-1 receptor accessory protein modulates neuronal responses to interleukin-1. Immunity *30*, 817–831. https://doi.org/10.1016/j.immuni.2009.03.020.

Snyder, G.A., Deredge, D., Waldhuber, A., Fresquez, T., Wilkins, D.Z., Smith, P.T., Durr, S., Cirl, C., Jiang, J.S., Jennings, W., et al. (2014). Crystal structures of the Toll/interleukin-1 receptor (TIR) domains from the Brucella protein TcpB and host adaptor TIRAP reveal mechanisms of molecular mimicry. J. Biol. Chem. *289*, 669–679. https://doi.org/10.1074/jbc.m113.523407.

Tao, X., Xu, Y.W., Zheng, Y., Beg, A.A., and Tong, L. (2002). An extensively associated dimer in the structure of the C713S mutant of the TIR domain of human TLR2. Biochem. Biophys. Res. Commun. *299*, 216–221. https://doi.org/10.1016/s0006-291x(02)02581-0.

Thomas, C., Bazan, J.F., and Garcia, K.C. (2012). Structure of the activating IL-1 receptor signaling complex. Nat. Struct. Mol. Biol. *19*, 455–457. https://doi.org/10.1038/nsmb.2260.

Toshchakov, V.Y., and Neuwald, A.F. (2020). A survey of TIR domain sequence and structure divergence. Immunogenetics *72*, 181–203. https://doi.org/10.1007/s00251-020-01157-7.

Toshchakov, V.Y., Szmacinski, H., Couture, L.A., Lakowicz, J.R., and Vogel, S.N. (2011). Targeting TLR4 signaling by TLR4 Toll/IL-1 receptor domain-derived decoy peptides: identification of the TLR4 Toll/IL-1 receptor domain dimerization interface. J. Immunol. *186*, 4819–4827. https://doi.org/10.4049/jimmunol.1002424.

Tsutsumi, N., Kimura, T., Arita, K., Ariyoshi, M., Ohnishi, H., Yamamoto, T., Zuo, X., Maenaka, K.,

Park, E.Y., Kondo, N., et al. (2014). The structural basis for receptor recognition of human interleukin-18. Nat. Commun. *5*, 5340. https://doi.org/10.1038/ncomms6340.

Valkov, E., Stamp, A., Dimaio, F., Baker, D., Verstak, B., Roversi, P., Kellie, S., Sweet, M.J., Mansell, A., Gay, N.J., et al. (2011). Crystal structure of Toll-like receptor adaptor MAL/TIRAP reveals the molecular basis for signal transduction and disease protection. Proc. Natl. Acad. Sci. U S A *108*, 14879–14884. https://doi.org/10.1073/pnas.1104780108.

Ve, T., Vajjhala, P.R., Hedger, A., Croll, T., DiMaio, F., Horsefield, S., Yu, X., Lavrencic, P., Hassan, Z., Morgan, G.P., et al. (2017). Structural basis of TIR-domain-assembly formation in MAL- and MyD88-dependent TLR4 signaling. Nat. Struct. Mol. Biol. *24*, 743–751. https://doi.org/10.1038/nsmb.3444.

Ve, T., Williams, S.J., and Kobe, B. (2015). Structure and function of Toll/interleukin-1 receptor/resistance protein (TIR) domains. Apoptosis *20*, 250–261. https://doi.org/10.1007/s10495-014-1064-2.

Vigers, G.P., Anderson, L.J., Caffes, P., and Brandhuber, B.J. (1997). Crystal structure of the type-I interleukin-1 receptor complexed with interleukin-1β. Nature *386*, 190–194. https://doi.org/10.1038/386190a0.

Vyncke, L., Bovijn, C., Pauwels, E., Van Acker, T., Ruyssinck, E., Burg, E., Tavernier, J., and Peelman, F. (2016). Reconstructing the TIR side of the myddosome: a paradigm for TIR-TIR interactions. Structure *24*, 437–447. https://doi.org/10.1016/j.str.2015.12.018.

Wan, L., Essuman, K., Anderson, R.G., Sasaki, Y., Monteiro, F., Chung, E.H., Osborne Nishimura, E., DiAntonio, A., Milbrandt, J., Dangl, J.L., and Nishimura, M.T. (2019). TIR domains of plant immune receptors are NAD(+)-cleaving enzymes that promote cell death. Science *365*, 799–803. https://doi.org/10.1126/science.aax1771.

Wang, D.L., Zhang, S.Y., Li, L.A., Liu, X., Mei, K.R., and Wang, X.Q. (2010). Structural insights into the assembly and activation of IL-1 beta with its receptors. Nat. Immunol. *11*, 905–911. https://doi.org/10.1038/ni.1925.

Wei, H., Wang, D.L., Qian, Y., Liu, X., Fan, S.L., Yin, H.S., and Wang, X.Q. (2014). Structural basis for the specific recognition of IL-18 by its alpha receptor. FEBS Lett. *588*, 3838–3843. https://doi.org/10.1016/j.febslet.2014.09.019.

Williams, S.J., Sohn, K.H., Wan, L., Bernoux, M., Sarris, P.F., Segonzac, C., Ve, T., Ma, Y., Saucet, S.B., Ericsson, D.J., et al. (2014). Structural basis for assembly and function of a heterodimeric plant immune receptor. Science *344*, 299–303. https://doi.org/10.1126/science.1247357.

Xu, Y., Tao, X., Shen, B., Horng, T., Medzhitov, R., Manley, J.L., and Tong, L. (2000). Structural basis for signal transduction by the Toll/interleukin-1 receptor domains. Nature *408*, 111–115. https://doi.org/10.1038/35040600.

Yabuuchi, K., Minami, M., Katsumata, S., and Satoh, M. (1994). Localization of type I interleukin-1 receptor mRNA in the rat brain. Mol. Brain Res. *27*, 27–36. https://doi.org/10.1016/0169-328x(94)90180-5.

Zhang, X.X., Bernoux, M., Bentham, A.R., Newman, T.E., Ve, T., Casey, L.W., Raaymakers, T.M., Hu, J., Croll, T.I., Schreiber, K.J., et al. (2017). Multiple functional self-association interfaces in plant TIR domains. Proc. Natl. Acad. Sci. U S A *114*, E2046–E2052. https://doi.org/10.1073/pnas.1621248114.

STAR★METHODS

KEY RESOURCES TABLE

REAGENT or RESOURCE	SOURCE	IDENTIFIER
Antibodies		
Rabbit Anti-IL-1RAcP Antibody	Rockland	Cat# 600-401-BV3
Rabbit Monoclonal Anti-IL-1RAcP Antibody	AbCam	Cat# ab256461
Mouse Monoclonal Anti-GAPDH Antibody	HuaXing Bio	Cat# HX1828
Anti-rabbit IgG, HRP-linked Antibody	CST	Cat# 7074S
HRP-Goat Anti-Mouse IgG (H+L)	HuaXing Bio	Cat# HX2032
Chemicals, peptides, and recombinant proteins		
IL-1RAcPb-TIR	This paper	N/A
IL-18Rβ-TIR	This paper	N/A
IL-1RAPL2-TIR	This paper	N/A
zSIGIRR-TIR	This paper	N/A
zSIGIRR-C299S-TIR	This paper	N/A
IL-1β mature	This paper	N/A
Critical commercial assays		
Dual-Luciferase Reporter Assay Kit	Vigorous Bio	Cat# T002
ABclonal MultiF Seamless Assembly Mix kit	ABclonal	Cat# RK21020
TIANprep Mini Plasmid Kit	TIANGEN	Cat# DP103
EndoFree Maxi Plasmid Kit	TIANGEN	Cat# DP117
Deposited data		
IL-1RAcPb-TIR	This paper	7FCC
IL-18Rβ-TIR	This paper	7FCH
IL-1RAPL2-TIR	This paper	7FD3
zSIGIRR-TIR	This paper	7FCL
zSIGIRR-C299S-TIR	This paper	7FCJ
Experimental models: Cell lines		
293T-IL-1RAcP-KO	Ge et al. (2019)	https://www.cell.com/structure/fulltext/S0969-2126(19)30173-X
Recombinant DNA		
pGL3/NF-kB-luc	Zhijie Chang's Lab	http://www.jbc.org/content/290/2/861.long
pRL-TK	Zhijie Chang's Lab	http://www.jbc.org/content/290/2/861.long
Software and algorithms		
HKL2000	Otwinowski and Minor (1997)	https://www.hkl-xray.com/hkl-2000
Phaser-MR	McCoy et al. (2007)	https://phenix-online.org/
Coot	Emsley et al. (2010)	https://www2.mrc-lmb.cam.ac.uk/personal/pemsley/coot/
Phenix Refine	Afonine et al. (2012)	https://phenix-online.org/
PyMol	Janson et al. (2017)	https://pymol.org/2/
AlphaFold2	Callaway (2021)	https://www.alphafold.ebi.ac.uk/

RESOURCE AVAILABILITY

Lead contact

Further information and requests for resources and reagents should be directed to and will be fulfilled by the lead contact, Xinquan Wang (xinquanwang@mail.tsinghua.edu.cn).

Materials availability

This study did not generate new unique reagents.

Data and code availability

- Data

Structural data have been deposited at the Protein Data Bank and are publically available as of the date of publication. Accession numbers are listed in the key resources table.

All other data reported in this paper will be shared by the lead contact upon request.

- Code

This paper does not report original code.

- Additional information

Any additional information required to reanalyze the data reported in this paper is available from the lead contact upon request.

EXPERIMENTAL MODEL AND SUBJECT DETAILS

Escherichia coli BL21 (DE3) cells used for IL-1R TIR domains and IL-1β recombinant proteins expression were cultured in LB media at 37°C; the cells were induced with 0.5 mM IPTG at 16°C for 18–19 h. 293T-IL-1RAcP-KO cells were used to perform *in vitro* Luciferase reporter assays, which were cultured in DMEM with 10% fetal bovine serum (FBS) and incubated at 37°C in a humidified atmosphere of 5% CO_2.

METHOD DETAILS

Plasmid construction

The coding sequences of following TIR domains, IL-1RAcP-TIR (residues 403–550), IL-1RAcPb-TIR (residues 403–548), IL-18Rβ-TIR (residues 406–562), IL-1RAPL2-TIR (residues 400–560), zSIGIRR-TIR (residues 180–327) and zSIGIRR-C299S-TIR (residues 180–327), were cloned into pET-22b vector (Invitrogen) with a C-terminal 6×His tag. cDNAs for human full-length IL-1RAcP (residues 1–570), IL -1RAcPb (residues 1–687) and a series of related mutants were cloned into pcDNA3.1(+) vector (Invitrogen). Swap mutations and point mutations were introduced by overlapping PCR. Briefly, the upstream and downstream primers containing sequences homologous to both the pcDNA3.1(+) vector and/or the mutated target cDNA fragment were used in PCR amplification reaction with IL-1RAcP or IL-1RAcPb as the template. The products were then ligated with the linearized vectors to obtain the mutants. Human IL-1β was cloned into the pGEX6p-1 vector with a GST tag at the N-terminus, that is, mature IL-1β (residues 117–269) cDNA fragment was inserted into the multiple cloning site of pGEX6p-1 plasmid. All these constructs were generated using 2×MultiF Seamless Assembly Mix (ABclonal) and sequence verified.

Protein expression and purification

All the TIR domain proteins were expressed and purified with a similar procedure as below. Firstly, the proteins tagged with 6×His were overexpressed in *Escherichia coli* BL21 (DE3) cultured in LB medium, which were induced with 0.5 mM isopropyl-β-D-thiogalactopyranoside at 16°C overnight. The cells were collected by centrifugation at 3,725 × g for 20 min, and resuspended with HBS buffer [10 mM Hepes (pH 7.2), 150/500 mM NaCl], and further disrupted by an EmulsiFlex-C3 homogenizer (Avestin) to release the target proteins. The lysate was centrifuged at 23,000 × g for 1 h, and the soluble target proteins within the supernatant were attached by Ni-NTA affinity column. Next, the column was subjected to extensive washing with HBS buffer supplemented with 20 mM imidazole. The proteins were eluted with HBS buffer supplemented with 250 mM imidazole, then concentrated and further purified by gel filtration chromatography on a Superdex 75 10/300 column (GE Healthcare) using the AKTA Purifier 10 system. Purified peak fractions could be utilized for next step assay directly, or pooled, concentrated, aliquoted, flash frozen by liquid nitrogen and stored at −80°C for future use. During the whole purification process, the target proteins were always in the HBS (150 mM NaCl) buffer containing 10 mM Hepes (pH7.2) and 150 mM NaCl, except for IL-18Rβ-TIR and IL-1RAPL2-TIR, which were dissolved in the HBS (500 mM NaCl) buffer containing 10 mM Hepes (pH 7.2) and 500 mM NaCl.

The mature form of human cytokine IL-1β (residues 117–269) was expressed and purified similar to TIR domains. In brief, the IL-1β was expressed with the pGEX-6P-1 vector in *Escherichia coli* strain BL21 (DE3). IL-1β with an N-terminal glutathione S-transferase tag was collected with Glutathione Sepharose 4 Fast Flow (GE Healthcare), followed by digestion with PreScission protease (GE Healthcare) for removal of the tag and further purification by gel-filtration chromatography.

Crystallization and diffraction data collection

The purified TIR domain proteins retaining the 6×His tag at the C-terminus were concentrated to about 10 mg/mL for initial screening of crystallization conditions, respectively. The crystals were prepared at 18°C via the vapor diffusion method in sitting drops composed of 100 nL protein solution (target proteins in its corresponding purification buffer) and 100 nL reservoir solution. The initial protein crystallization conditions were identified by sparse matrix screening of commercial crystallization kits (Hampton Research), followed by extensive optimization, in which the sitting and the hanging drop methods were both utilized. The optimal reservoir solution conditions and the suitable protein concentrations were finally screened out and listed as follows: 0.1 M sodium citrate, pH 5.6, 20%w/v PEG4000, 20% v/v 2-propanol for IL-1RAcPb-TIR (6.7 mg/mL); 0.2 M ammonium tartrate dibasic, pH 6.25, 20% w/v PEG3350, 3% v/v (+/−)-2-methyl-2,4-pentanediol for IL-18Rβ-TIR (9.86 mg/mL); 8% v/v tacsimate pH5.0, 12% w/v PEG3350 for IL-1RAPL2-TIR (19.3 mg/mL); 0.05 M ammonium sulfate, 0.05 M Bis-Tris pH6.9, 34% v/v pentaerythritol ethoxylate (15/4 EO/OH), 3% v/v glycerol for zSIGIRR-TIR (22.5 mg/mL) and 0.1 M CHES pH 9.5, 20% w/v PEG8000 for zSIGIRR-C299S-TIR (14 mg/mL). The crystals were first briefly soaked in cryoprotectant that was composed of reservoir solution supplemented with ~25% (v/v) glycerol, and then flash frozen in liquid nitrogen for data collection. All X-ray diffraction data sets were collected at BL-17U1 beamline of the Shanghai Synchrotron Radiation Facility (SSRF) using the light wavelength of 0.9794 angstroms under the condition of −196°C, and next indexed and integrated with the program HKL2000 (Otwinowski and Minor, 1997). The statistics of data processing are summarized in Table 1.

Structure determination and refinement

The initial phases of IL-1RAPL2-TIR and IL-1RAcPb-TIR were determined by molecular replacement method using the crystallographic software PHASER (McCoy et al., 2007) in the CCP4 suite with the published crystal structure of IL-1RAPL1-TIR (PDB ID: 1T3G) as the search model. Then the molecular replacement solutions of IL-18Rβ-TIR and zSIGIIRR-C299S-TIR were determined using IL-1RAcPb-TIR structure as the search model. Finally, the solution of zSIGIRR-TIR was determined with zSIGIIRR-C299S-TIR structure as the template. Subsequently, iterative refinement and model building were performed with the program PHENIX (Afonine et al., 2012) and COOT (Emsley et al., 2010), respectively. The structure refinement statistics are also summarized in Table 1. All structure figures were generated using PyMol (Janson et al., 2017).

Dual-luciferase report assays

To detect IL-1-mediated NF-κB signal transduction, the IL-1RAcP knockout HEK293T cells (293T-IL-1RAcP-KO cell line (Ge et al., 2019)) were uniformly seeded in Costar White 24-well plates (0.5×10^6 cells/mL) prior to transfection. The cell culture medium was DMEM containing 10% fetal bovine serum (FBS) and 1×penicillin (PS). The IL-1RAcP/IL-1RAcPb receptors or their mutants, whose cDNA sequences were made C726G synonymous mutation to avoid Cas9 cleavage and cloned into the pcDNA3.1 vector, were transiently co-transfected with pGL3/NF-κB-luc and pRL-TK into the cells after 12 h. pGL3/NF-κB-luc was used as IL-1 signaling reporter vector, in which a human NF-κB promoter was located prior to the firefly luciferase coding sequence; the pRL-TK reporter vector was used to normalize the transfection efficiency, in which a constitutively active promoter was located just before Renilla luciferase coding region. Specifically, 200 ng/well receptor plasmids, 60 ng/well pGL3/NF-κB-luc, and 5 ng/well pRL-TK were mixed and enveloped with PEI at a mass ratio of 1:4. It was then added dropwise into the well after standing for 25 min at room temperature. All wells were transfected with the same amount of plasmid. Besides, the equivalent amount of pcDNA3.1 empty vector plasmid was used in the negative control group. 12 h post-transfection, the medium was substituted by fresh DMEM without FBS and PS, and the cells were starved for another 12 h. Then cells in half of the wells were stimulated with IL-1β cytokine at a titrated concentration of 5 nM for 7 h. Next, the luciferase activity was detected with the dual-luciferase reporter kit (Vigorous bio) in the plate reader Centro LB960, which proceeded according to the following steps: removing the medium from the wells, gently washing the wells twice with an appropriate amount of 1×PBS buffer, adding 120 μL 1×lysis buffer, shaking for 20 min at room temperature to lyse the cells completely, and transferring 20 μL lysate into the reading plate for firefly luciferase and Renilla luciferase activity measurement with the addition

of substrate 1 and substrate 2. The substrates were protected from light. The IL-1β-triggered signal values of firefly luciferase were normalized against those of Renilla luciferase for transfection efficiency and plotted as fold stimulation over the unstimulated control. In addition, the corresponding cell lysates were used for western blot to quantify protein expression levels. All the experiments were conducted in triplicate.

Western blot

All samples ready for western blotting were dissolved in 5×SDS loading buffer (50 mM Tris, 2% SDS, 0.1% bromophenol blue, 50% glycerol, 100 mM DDT), and then separated by gel electrophoresis with SurePAGE, Bis-Tris, 10 × 8 gels (GenScript) in the 1×Tris-MOPS-SDS Runing Buffer (GenScript). Next, proteins were transferred onto the nitrocellulose membranes (Bio-Rad). To detect proteins of IL-1RAcP/IL-1RAcPb or their mutants, rabbit anti-IL-1RAcP (Rockland, ABcam) was used as the primary antibody, and anti-rabbit IgG, HRP-linked antibody (Cell Signaling Technology) as the secondary antibody. Immunoblotting data were collected using the machine of Amersham Imager 600 (GE Health).

QUANTIFICATION AND STATISTICAL ANALYSIS

For Luciferase reporter assays, data was plotted using Origin 9.1. Pooled data from N = 3 separate experiments and Standard Deviation (SD) is shown.